CATALYTIC TRANSFORMATION OF OXYGEN CONTAINING COMPOUNDS INTO VALUABLES: EFFECT OF CERIA REDOX PROPERTIES

Kamil Mustafin

Submitted for the degree of Master of Philosophy

Heriot-Watt University

School of Engineering and Physical Sciences

February 2018

Abstract

The focus of this thesis is the investigation of sustainable routes for the production of commercially valuable oxygen containing compounds through the application of ceria-based catalysts. The catalytic transformation of levulinic acid (to γ-valerolactone), CO_2, methanol and nitrobenzene (to methyl-N-phenyl carbamate), 1-butanol (to 1-butene) and 1,3-butanediol (to 3-buten-2-ol) have been examined. Taking the conversion of levulinic acid as a model system, it was established that the surface oxygen vacancies, formed during temperature programmed reduction of reducible oxides, activate levulinic acid for reaction. Process sustainability has been examined in terms of full hydrogen utilisation with 100% yield of the target γ-valerolactone under stoichiometric conditions over supported Au catalysts. The production of the carbamate directly from CO_2 was initially optimised towards dimethyl carbonate formation as a reaction intermediate, where the highest reported rate has been achieved. It was shown that total surface area of CeO_2 is not a determining parameter for catalytic performance, while a decrease in Ce^{3+} content upon calcination improves CO_2 activation. Dehydration of 1-butanol/1,3-butanediol revealed the requirement for the strong Lewis acid sites on the surface of the catalyst to form an alkene. The results presented in this thesis demonstrate direct participation of the ceria in the catalytic dehydration and carboxylation reactions.

Dedication

To my wonderful family

Irade Mustafina and Farid Mustafin

Nailya Mustafina and Yury Kovtun

Table of Contents

List of Tables

List of Figures

Glossary

Acronyms

1,3-BD	1,3-Butanediol
2B1OL	2-Buten-1-ol
3B1OL	3-Buten-1-ol
3B2OL	3-Buten-2-ol
AAS	Atomic Absorption Spectroscopy
AGL	α-Angelica Lactone
AN	Aniline
BD	Butadiene
BE	Binding Energy
DMC	Dimethyl Carbonate
FID	Flame Ionisation Detector
GHSV	Gas Hourly Space Velocity
GVL	γ-Valerolactone
HPA	Hydroxypentanoic Acid
i.d.	Internal Diameter, mm
JCPDS-ICDD	Joint Committee on Powder Diffraction Standards – International Centre for Diffraction Data
LA	Levulinic Acid
LWA	Lewis Acid
LWB	Lewis Base
MPC	Methyl N-Phenyl Carbamate
NB	Nitrobenzene
SSA	Specific Surface Area
STEM	Scanning Transmission Electron Microscopy
TCD	Thermal Conductivity Detector
TPD	Temperature Programmed Desorption
TPR	Temperature Programmed Reduction
XPS	X-ray Photoelectron Spectroscopy
XRD	Powder X-ray Diffraction

Symbols

d	Metal nanoparticle mean size, nm
F	Inlet organic reactant feed rate, mol h^{-1}
k	Kinetic rate constant, h^{-1}
L_{bed}	Catalyst bed length, mm
n	Moles of metal in the catalyst bed, mol
P	Pressure, atm
R	Reaction rate
R_0	Initial reaction rate
S_j	Selectivity to product "j", %
T	Reaction temperature, K
T_{max}	Temperature maximum in catalyst activation by TPR, K
V_{bed}	Catalyst bed volume, mm^3
X	Fractional conversion
X_0	Initial fractional conversion
X_{3h}	Fractional conversion after 3h time-on-stream
β	Time scale fitting parameter
τ	Contact time

List of Publications:

[1] K. Mustafin, F. Cárdenas-Lizana and M. A. Keane, *Continuous Gas Phase Catalytic Transformation of Levulinic Acid to γ-Valerolactone over Supported Au Catalysts*. J. Chem. Technol. Biotechnol., 2017. **92**: p. 2221-2228.

List of Presentations:

[1] Oral presentation at SURCAT ECOSSE Conference, Glasgow (2016)

Chapter 1

Introduction and Scope of the Thesis

This chapter provides an overview of the concept of sustainable chemical processes, focusing on the ceria-based catalysis. The objectives of this MPhil research are defined and the approach taken is described.

1.1 Sustainable Chemical Processing and production of oxygenated compounds

The chemical industry is heavily based on the exploitation of (*non*-renewable) fossil fuels for the production of a wide range of commodity chemicals [1]. The demand for the production of these chemicals has been increasing over the years, where the current global manufacture is more than 3.5×10^8 tonnes·year^{-1} with a prospect increase of 25% by 2020 [2]. Currently, hazardous feedstocks (e.g. highly flammable solvents, phosgene, volatile amines, isocyanates, etc.) [3] are used as raw materials to manufacture oxygen containing commodity chemicals, which are then used to produce fuel-additives, perfumes, solvents and pharmaceuticals [4, 5]. The use of these toxic feedstocks causes serious safety and environmental issues. Moreover, the conventional multistep route for the manufacture of commodities [6] results in the generation of large amounts of waste that requires treatment prior to disposal. These issues have stimulated the development of sustainable manufacturing processes, which need to involve a high degree of energy efficiency and circumvent the formation of by-products. Ceria-based catalysts have been proven to be effective in the production of chemical commodities due to their enhanced activity, selectivity and stability in various applications. Cerium oxide has been employed in a series of processes, *i.e.* direct synthesis of carbonates [7], selective hydrogenation [8, 9], reactions involving aldol condensations [10] and others. In most cases, the redox properties of ceria-based catalysts are considered to play a key role in determining their catalytic behaviour [11]. However, it is crucial and essential to further optimise this reaction system and improve the understanding of the structure-

property relationship of ceria-based catalysts in order to meet the requirements of sustainable chemical processing.

1.2 Scope and organisation of the thesis

The aim of this research was to explore the catalytic activity/selectivity and the redox properties of ceria-based catalysts for the synthesis of commercially valuable products. The work involved kinetic and thermodynamic analysis, catalyst preparation, characterisation and process optimisation. Catalyst characterisation has involved AAS, TPR, $H_2/O_2/NH_3$ chemisorption, H_2/CO_2 TPD, SSA, XRD, STEM and XPS measurements. A switch from batch liquid to continuous mode of operation offers the possibility to improve product quality, decrease energy consumption, solvent utilization and the amount of waste generated [3]. Ceria-based catalysts were employed in the production of oxygen containing compounds in **Chapter 2-5**; thesis organisation and scope are summarised in **Table 1.1**.

Table 1. 1: Scope of the studies undertaken in this thesis.

	Reactant	Catalysts	Objective
Chapter 2	Levulinic acid	Au/Al_2O_3 Au/CeO_2 Au/TiO_2 Pd/Al_2O_3	**Reducibility of the support, oxygen vacancies, exclusive production of the target γ-valerolactone**
Chapter 3	CO_2; H_2; N_2; methanol; nitrobenzene; aniline	CeO_2 Pd/CeO_2	**The role of support redox and acidity properties, the effect of CO_2 partial pressure, CeO_2 catalyst synthesis**
Chapter 4	1-butanol / 1,3-butanediol	CeO_2 Au/CeO_2 Ag/CeO_2 Pd/CeO_2	**Thermodynamic analysis, the role of support redox and acidity properties, the effect of metal incorporation**

The continuous gas phase transformation of Levulinic acid (LA) was examined over supported (Al_2O_3, CeO_2 and TiO_2) Au and catalytic performance compared with

benchmark Pd/Al_2O_3. Support reducibility facilitated the sequential hydrogenation and dehydration reactions providing additional active sites for LA activation. This work is extended in **Chapter 3**, where the effect of modifying the surface Ce^{3+} and Ce^{4+} of CeO_2 (by metal incorporation or calcination treatment) has been investigated on CO_2 activation in the carbamate synthesis. An influence of the redox properties of CeO_2 on product distribution along with mechanisms involved is further examined in 1-butanol/1,3-butanediol dehydration, comparing the catalytic action of ceria supported Au, Ag and Pd systems in **Chapter 4**. The thesis ends (**Chapter 5**) with a concluding summary and suggested future work.

1.3 References

[1.1] R. Sheldon, *Green and Sustainable Manufacture of Chemicals from Biomass: State of the Art*. Green Chem., 2014. **16**: p. 950-963.

[1.2] Y. Yao, D. Graziano, M. Riddle, J. Cresko and E. Masanet, *Greener Pathways for Energy-Intensive Commodity Chemicals: Opportunities and Challenges*. Curr. Opin. Chem. Eng., 2014. **6**: p. 90-98.

[1.3] A. Cybulski, J. Moulijn, M. Sharma and R. Sheldon, *Chapter 1 – Introduction, In Fine Chemicals Manufacture*. Elseiver Science B.V., 2001: p. 1-13.

[1.4] A. Cornejo, I. Barrio, M. Campoy, J. Lázaro and B. Navarrete, *Oxygenated Fuel Additives from Glycerol Valorization. Main Production Pathways and Effects on Fuel Properties and Engine Performance: A Critical Review*. Renew. Sust. Energ. Rev., 2017. **79**: p. 1400-1413.

[1.5] R. Breitling and E. Takano, *Synthetic Biology Advances for Pharmaceutical Production*. Curr. Opin. Biotech., 2015. **35**: p. 46-51.

[1.6] A. Halpaap and J. Dittkrist, *Sustainable Chemistry in the Global Chemicals and Waste Management Agenda*. Curr. Opin. Green Sust. Chem., 2018. **9**: p. 25-29.

[1.7] H.J. Lee, S. Park, I.K. Song and J.C. Jung, *Direct Synthesis of Dimethyl Carbonate from Methanol and Carbon Dioxide over $Ga_2O_3/Ce_{0.6}Zr_{0.4}O_2$ Catalysts: Effect of Acidity and Basicity of the Catalysts*. Catal. Lett., 2011. **141**: p. 531-537.

[1.8] F. Cárdenas-Lizana, Z.M. de Pedro, S. Gómez-Quero and M.A. Keane, *Gas Phase Hydrogenation of Nitroarenes: A Comparison of the Catalytic Action of Titania Supported Gold and Silver*. J. Molec. Catal. A, Chem., 2010. **326**: p. 48-54.

[1.9] L. McEwan, M. Julius, S. Roberts and J.C.Q. Fletcher, *A Review of the Use of Gold Catalysts in Selective Hydrogenation Reactions*. Gold Bull., 2010. **43**: p. 298-306.

[1.10] G. Postole, B. Chowdhury, B. Karmakar, K. Pinki, J. Banerji and A. Auroux, *Knoevenagel Condensation Reaction over Acid–Base Bifunctional Nanocrystalline $Ce_xZr_{1-x}O_2$ Solid Solutions*. J. Catal., 2010. **269**: p. 110-121.

[1.11] J.J. Delgado, E. del Río, X. Chen, G. Blanco, J.M. Pintado, S. Bernal and J. J. Calvino, *Understanding Ceria-Based Catalytic Materials: An Overview of Recent Progress*. Catalysis by Ceria and Related Materials, 2013. **2**: p. 47-138.

Chapter 2

Continuous Gas Phase Catalytic Transformation of Levulinic Acid to γ-Valerolactone over Supported Au Catalysts

γ-Valerolactone is a high value chemical obtained from hydrogenation of bio-derived levulinic acid. In this chapter, the role of support redox and acidity properties has been examined in the continuous gas phase hydrogenation of aqueous levulinic acid at ambient pressure over gold on Al_2O_3, CeO_2 and TiO_2; Pd/Al_2O_3 served as a benchmark in catalyst tests. This chapter has been published in Journal of Chemical Technology and Biotechnology. Co-authors F.C.-L. and M.A.K. directed the project and co-wrote the chapter.

2.1 Introduction

γ-Valerolactone (GVL) is a lignocellulose building block chemical used as an intermediate in alkane (jet fuel, gasoline and diesel fuel), aromatic (fuel additives), polymer and solvent production [1]. The main route to GVL is the hydrogenation of levulinic acid (LA), obtained from cellulose, starch, or C6 sugars [2] *via* low cost (\$0.09-0.22 kg^{-1}) acid hydrolysis [3, 4]. The reaction pathways from a compilation of the literature [5-7] on LA → GVL transformation are presented in **Figure 2.1**. GVL production proceeds *via* hydrogenation and dehydration steps. The predominant pathway is still a matter of debate where variations in operating conditions [5], choice of support [8] and metal [9] or solvent [10] impacts on catalytic activity and/or selectivity.

The catalytic hydrogenation of LA using both homogeneous [11] and heterogeneous [5] systems has been investigated. Heterogeneous catalysis offers advantages in terms of product separation and catalyst reuse. Work to date has largely dealt with pressurised (5-250 bar) batch liquid phase conversion in organic solvents (1,4-dioxane, methanol and toluene) where full selectivity to GVL at high conversions remains challenging [11-14].

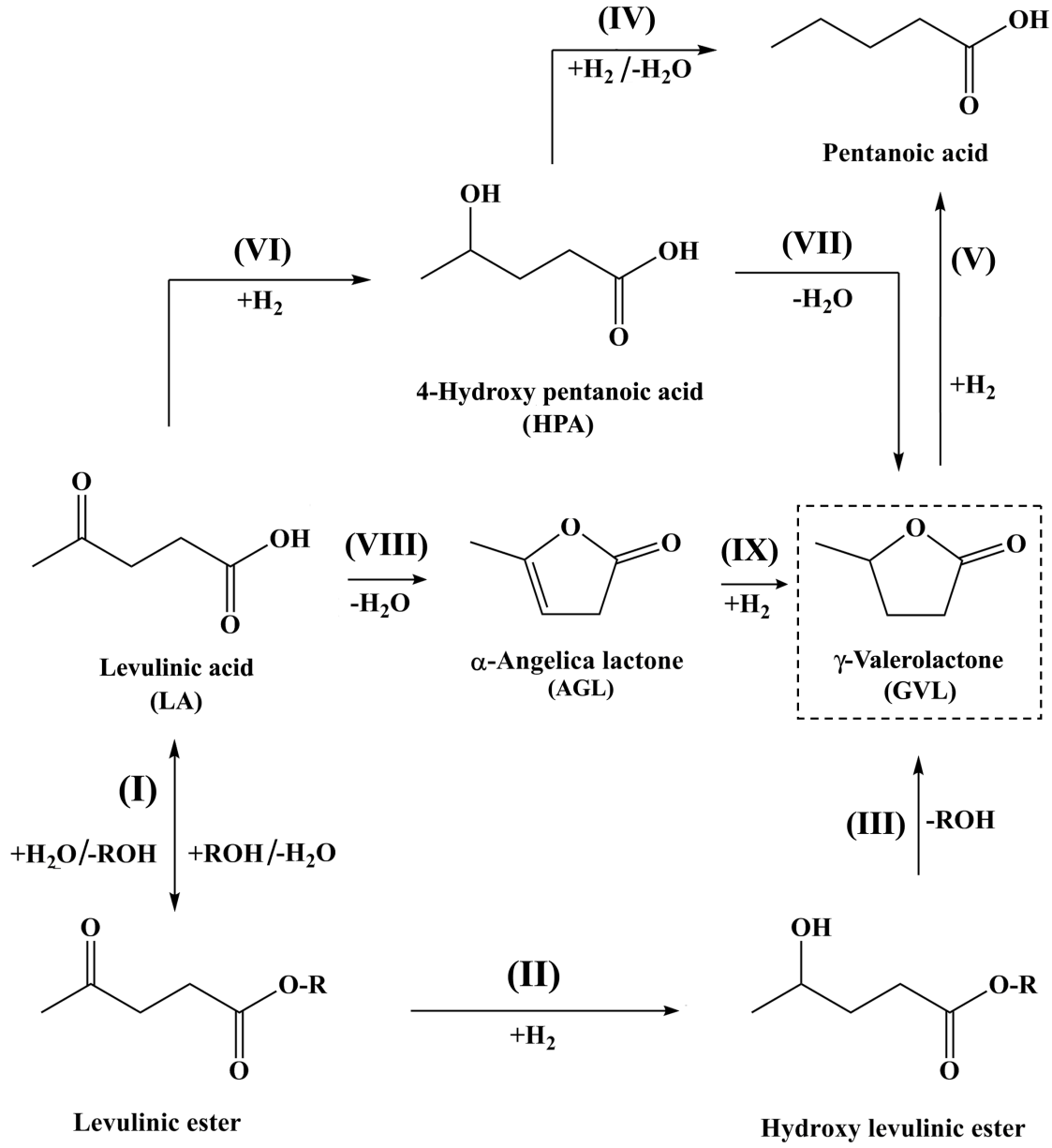

Figure 2. 1: Reaction pathways involved in the transformation of levulinic acid (LA) to the target (framed) *γ*-valerolactone (GVL).

Continuous GVL formation at ambient pressure facilitates higher throughput. In catalytic hydrogenation, control over contact time can govern conversion [15] and selectivity [16]. Reviews by Wright and Palkovits in 2012 [5], Yan *et al.* in 2015 [7] and Delidovich *et al.* in 2016 [17] identified supported Pd and Ru as the best catalysts for continuous gas phase transformation of LA with a productivity of 81-91 $mmol_{GVL}$

g_{metal}^{-1} h^{-1} and 90-98.6% GVL yield. Use of toxic 1,4-dioxane [18] as solvent and excess hydrogen are process sustainability issues to be addressed.

The use of supported gold catalysts for the transformation of biomass-derived feedstock to value-added chemicals is showing promise [19]. Notable examples include aldehyde reduction (*e.g.* 2-hydroxymethyl-5-furfural → 2,5-bis(hydroxymethyl)furan) [20], dehydration of carbohydrates [21] and hydrogenation/dehydration of succinic anhydride to γ-butyrolactone [22]. Lewis and Brønsted acid sites contribute to catalytic dehydration [23] (**Figure 2.1**, steps **(I)**, **(IV)**, **(VII)**, and **(VIII)**). In the case of reducible oxide supports (*e.g.* titania and ceria), oxygen vacancies generated by the loss of structural oxygen from the oxide sub-lattice [24] can modify reactant adsorption/activation and influence catalytic performance [25]. These vacancies can fix oxygen in water [26], alcohols [27] and aldehydes [28]. Increased rate and carbonyl reduction selectivity in the conversion of aldehydes has been ascribed to facilitated -C=O activation at oxygen deficient sites in CeO_2 [29] and Fe_2O_3 [30]. Using DFT calculations, Baker *et al.* [31] identified oxygen vacancies in Pd/TiO_2 as the catalytically active sites for -C=O reduction in furfural hydrogenation. The opposite effect is also possible where strong binding of oxygenated reactants to these vacancies [32] has been deemed responsible for lower hydrogenation activity [33].

In this work, we evaluate the impact of the support redox (reducibility) and acid properties in the continuous hydrogenation of LA over a series of oxide (Al_2O_3, CeO_2 and TiO_2) supported Au catalysts, taking Pd/Al_2O_3 as a benchmark. We examine the reaction pathways and consider the effect of varying inlet H_2/LA, using water as a solvent with a view to clean production of GVL.

2.2 Experimental

2.2.1 Catalyst Preparation and Activation

The oxide carriers (γ-Al_2O_3 (Puralox, Condea Vista Co.), CeO_2 (Grace Davison) and TiO_2 (P25, Degussa)) were used as received. Supported (1.0-3.0% wt.) Au catalysts were prepared by deposition-precipitation. Urea (100-fold excess, Riedel-de Haën, 99%), used as basification agent, was added to an aqueous solution of $HAuCl_4$ (4×10^{-5}

– 5×10^{-3} M; 20–50 cm^3, Sigma-Aldrich，99%) containing the support (5-30 g). The suspension was stirred and heated to 353 K (2 K min^{-1}) for 3 h in a He purge where the pH progressively increased to *ca.* 7 after 3 h as a result of thermally induced urea decomposition with Au^{3+} deposition [34]. The resultant solid was separated by centrifugation, washed with deionised water until the wash water was Cl-free ($AgNO_3$ test) and dried in He (45 cm^3 min^{-1}) at 373 K (2 K min^{-1}) for 5 h. A commercial Pd/Al_2O_3 (1.2% wt. Pd, Sigma-Aldrich) catalyst was employed as benchmark. Prior to use, the catalysts were sieved to 75 μm average particle diameter (ATM fine test sieves) and activated in 60 cm^3 min^{-1} H_2 at 2 K min^{-1} to 573–603 K. Samples were passivated in 1% v/v O_2/He at ambient temperature for *ex situ* analysis.

2.2.2 Catalyst Characterisation

The (Au and Pd) metal content was measured by atomic absorption spectroscopy (Shimadzu AA-6650 spectrometer with an air-acetylene flame) from the diluted extract in aqua regia (25% v/v HNO_3/HCl). Temperature programmed reduction (TPR), $H_2/O_2/NH_3$ chemisorption, temperature programmed desorption (TPD) and specific surface area (SSA) measurements were recorded using the commercial CHEM-BET 3000 (Quantachrome Instruments) unit equipped with a thermal conductivity detector (TCD) for monitoring gas composition and the TPR Win™ software for data acquisition/manipulation. Samples (0.05-0.1 g) were loaded into a U-shaped Quartz cell (3.76 mm i.d.), outgassed for 30 min and total SSA recorded in a 30% v/v N_2/He flow with undiluted N_2 (BOC, 99.9%) as internal standard. Two cycles of N_2 adsorption-desorption were employed using the standard single point BET method. TPR analysis was conducted in 17 cm^3 min^{-1} (Brooks mass flow controller) 5% v/v H_2/N_2 at 2 K min^{-1} to 573–603 K where the effluent gas passed through a liquid N_2 trap. Samples were maintained at the final isothermal hold in a flow of H_2/N_2 until the signal returned to baseline, swept with 65 cm^3 min^{-1} N_2 for 1.5 h, cooled to reaction (493 K, H_2 chemisorption) or ambient (NH_3 chemisorption) temperature and subjected to pulse (10-1000 μl) titration (BOC, ≥99.98%). Hydrogen/ammonia pulses were repeated until the signal area was constant and there was no detectable uptake. Ammonia TPD was conducted to determine total acidity [35]. Samples were thoroughly flushed in N_2 (65

cm^3 min^{-1}) for 1.5 h post-NH_3 titration to remove weakly bound NH_3 and heated at 30 K min^{-1} (in 65 cm^3 min^{-1} N_2) to 973 K. Oxygen chemisorption was performed to assess the extent of support reduction [36], where the samples were swept with 65 cm^3 min^{-1} He for 1.5 h post-TPR, cooled to 493 K and subjected to O_2 pulse (10 μl) titration. It has been demonstrated elsewhere that Au contribution to total O_2 adsorbed is negligible [37]. SSA and gas uptake values were reproducible to ±5%. Gold and Pd metal particle morphology (size and shape) was determined by scanning transmission electron microscopy (STEM) using a JEOL 2200FS operated at an accelerating voltage of 200 kV, employing Gatan Digital Micrograph 1.82 for data acquisition/manipulation. Samples for analysis were prepared by dispersion in acetone and deposited on a holey Cu grid (300 mesh). The number weighted mean Au and Pd diameters (*d*) were determined from a count of up to 800 particles [38].

2.2.3 Gas Phase Hydrogenation of Levulinic acid (LA)

2.2.3.1 Materials

LA (98%) and GVL (99%) were supplied by Sigma-Aldrich and used as received. All the gases (H_2, N_2, O_2 and He) were of ultra-high purity (BOC, ≥99.99%).

2.2.3.2 Catalytic System

Reactions were performed at ambient pressure over the temperature range 493-573 K, immediately after *in situ* catalyst activation in a fixed bed vertical continuous plug-flow glass reactor (i.d. = 12 mm). A layer of borosilicate glass balls (2 mm diameter; height = 3 cm) served as preheating zone, ensuring the reactant was vaporised and reached reaction temperature before contacting the catalyst. Isothermal conditions (±1 K) were maintained by diluting the catalyst bed (L_{bed} = 2 mm; V_{bed} = 226 mm^3; fraction of catalyst in the bed by volume = 0.1-1) with ground glass (75 μm). Reaction temperature was continuously monitored by a thermocouple inserted in a thermowell within the catalyst bed. An aqueous or organic (toluene) solution of LA (0.29 M) was delivered to the reactor *via* a glass/teflon air-tight syringe and a teflon line at a fixed calibrated flow rate using a microprocessor controlled infusion pump (Model 100, KD Scientific). A co-current flow of LA and H_2, N_2 or H_2+N_2 was maintained at $GHSV = 2 \times 10^4$ h^{-1} where inlet H_2/LA was varied from stoichiometry (=1 for GVL formation) to

far in excess (=420); gas flow rate was monitored using a Humonics (Model 520) digital flowmeter. The molar metal (n) to inlet LA feed rate (F) spanned the range $5 \times 10^{-4} - 1 \times 10^{-2}$ h. In a series of blank tests, reactions using GVL or LA as reactant in a stream of H_2 through the empty reactor or over the support alone did not result in any detectable conversion.

2.2.3.3 Analytical Method and Activity/Selectivity Evaluation

The reactor effluent was frozen in a liquid nitrogen trap and analysed by capillary GC (Perkin-Elmer Auto System XL gas chromatograph equipped with a programmed split/splitless injector and flame ionisation detector (FID)) using a Stabilwax (fused silica) 30 m × 0.32 mm i.d., 0.25 μm film thickness capillary column (RESTEK), employing Turbo-Chrom Workstation Version 6.3.2 (for Windows) for data storage and manipulation. Product composition was based on detailed calibration plots (not shown) using commercial samples. Catalytic activity is quantified in terms of fractional conversion (X)

$$X = \frac{\mathrm{LA_{in}} - \mathrm{LA_{out}}}{\mathrm{LA_{in}}} \qquad \textbf{(2.1)}$$

extracted from time on-stream measurements [39]. Selectivity in terms of the target GVL (S_{GVL}) is given by

$$S_{\mathrm{GVL}} = \frac{\mathrm{GVL_{out}}}{\mathrm{LA_{in}} - \mathrm{LA_{out}}} \times 100 \qquad \textbf{(2.2)}$$

where the subscripts "in" and "out" refer to the inlet and outlet streams. Repeated reactions with different samples from the same batch of catalyst delivered conversion/selectivity values reproducible to within ±5%; carbon mass balance was complete to better than ±9%.

2.3 Results and discussion

2.3.1 Catalyst Characterisation

Catalyst physico-chemical characteristics are given in **Table 2.1**. The SSA range from 52 $m^2\ g^{-1}$ (Au/TiO_2) to 166 $m^2\ g^{-1}$ (Au/Al_2O_3) and the values obtained for each system are in agreement with those reported in the literature [40, 41]. The TPR profiles

of laboratory synthesised Au/Al_2O_3 **(A)**, Au/CeO_2 **(B)** and Au/TiO_2 **(C)** are presented in **Figure 2.2(I)** with associated H_2 consumption in **Table 2.1**. Activation of Pd/Al_2O_3 by TPR followed the procedure described previously [42]. Au/Al_2O_3 exhibited a single positive peak at 461 K that is comparable with the literature [43].

Table 2. 1: Physico-chemical characteristics of supported Au and Pd catalysts and pseudo-first order rate constant for the transformation of levulinic acid to γ-valerolactone at 493 K (k_{493}).

Catalyst	Au/Al_2O_3	Au/CeO_2	Au/TiO_2	Pd/Al_2O_3
SSA ($m^2\ g^{-1}$)	166	108	52	156
TPR H_2 consumption $\times 10^2$ ($\mu mol\ g^{-1}$)	$1^a/1^b$	$5^a/2^b$	$2^a/1^b$	-
H_2 chemisorption ($\mu mol\ g^{-1}$)[c]	5	3	4	17
O_2 chemisorption $\times 10^{-2}$ ($\mu mol\ m^{-2}$)[c]	1	21	23	2
d (nm)	4.3	3.0	3.2	3.0
(NH_3 chemisorption[d] / TPD) $\times 10^{-2}$ ($mmol\ g^{-1}$)	15/16	23/28	12/12	-
k_{493} (h^{-1})	33	83	96	128

[a]experimentally determined value
[b]theoretical value for $Au^{3+} \rightarrow Au^0$
[c]titration at 493K
[d]titration at 298K

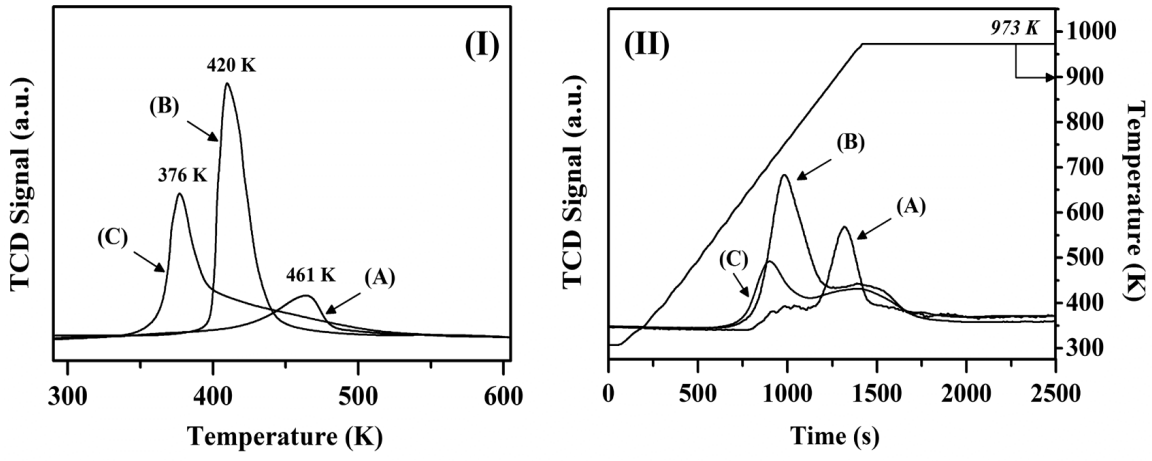

Figure 2. 2: (I) TPR and (II) NH_3-TPD profiles for (A) Au/Al_2O_3, (B) Au/CeO_2 and (C) Au/TiO_2.

Hydrogen consumption matched the requirements for $Au^{3+} \rightarrow Au^{0}$. A lower temperature reduction peak was in evidence for Au/CeO_2 (T_{max} = 420 K) and Au/TiO_2 (T_{max} = 376 K) and can be linked to weaker Au-support interactions [40] resulting in a more facile reduction of the metal phase [44]. Hydrogen consumption during TPR of Au/CeO_2 (5×10^2 μmol g^{-1}) and Au/TiO_2 (2×10^2 μmol g^{-1}) exceeded the amount required for reduction of the metal precursor (**Table 2.1**), indicative of partial support reduction [45]. Hydrogen chemisorption on all the Au catalysts was lower than the benchmark Pd/Al_2O_3 (**Table 2.1**), which can be explained by the higher activation barrier for dissociative H_2 adsorption on Au [46]. The consensus from the literature suggests that H_2 adsorption on Au is dependent on temperature and Au coordination [47]. Smaller Au particles exhibit a greater preponderance of corner and edge sites that facilitate H_2 adsorption, which is favoured by a higher titration temperature [48]. Dissociated H_2 chemisorbed on Au can spill onto the support and promote superficial reduction of the oxide carrier with the generation of oxygen vacancies, an effect that has been reported for Au/CeO_2 [49] and Au/TiO_2 [50].

Oxygen chemisorption post-TPR was negligible on Au/Al_2O_3 and Pd/Al_2O_3 (**Table 2.1**), consistent with the *non*-reducibility of Al_2O_3 where temperatures ≥1373 K are required for oxide reduction [51]. Greater uptake on Au/CeO_2 and Au/TiO_2 is consistent with vacancy formation during TPR of these reducible oxides. Representative STEM images **(I)** and associated particle size distribution histograms **(II)** for Au/Al_2O_3 **(A)**, Au/CeO_2 **(B)** and Au/TiO_2 **(C)** are provided in **Figure 2.3**. The Au particles are in the 1-8 nm size range, which has been identified as crucial for hydrogenation activity [52]. Au/CeO_2 and Au/TiO_2 showed a narrower distribution of smaller metal particles, which can be linked to stabilisation at oxygen vacancies that serves to inhibit sintering during TPR [53]. The Pd/Al_2O_3 sample exhibited similar mean metal size (**Table 2.1**) and is a suitable reference catalyst to assess the catalytic performance of supported Au in LA hydrogenation.

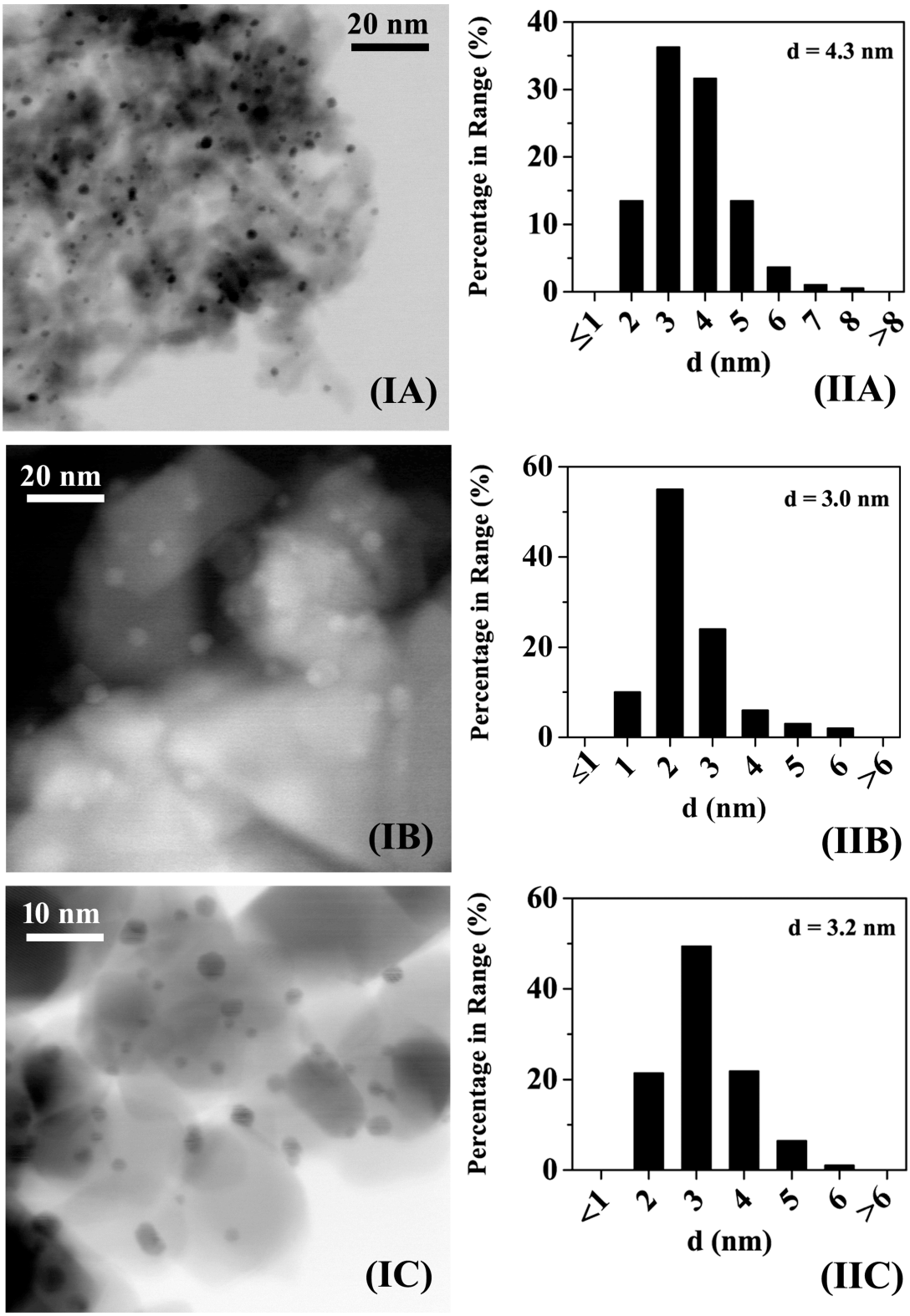

Figure 2. 3: Representative (I) STEM images and (II) associated Au particle size distributions for (A) Au/Al_2O_3, (B) Au/CeO_2 and (C) Au/TiO_2.

Surface acidity was determined by NH_3 chemisorption/TPD. Total acidity measurements coincided for titration and TPD; the desorption profiles for Au/Al_2O_3 **(A)**, Au/CeO_2 **(B)** and Au/TiO_2 **(C)** are provided in **Figure 2.2(II)**. The three catalysts exhibited a principal desorption peak for NH_3 release over the 600-973 K range, characteristic of strong acid sites, *i.e.* NH_3 desorption at $T \geq 673$ K [8, 54]. Surface acidity in the case of Al_2O_3, CeO_2 and TiO_2 is associated with uptake at Al^{3+}, Ce^{4+} or Ti^{4+} Lewis acid centres, as demonstrated by XPS [55], temperature-programmed redaction [55], NMR [56] and FT-IR [57, 58] measurements. The quantity of NH_3 chemisorbed/desorbed (**Table 2.1**) on the three Au catalysts ($12\text{-}28 \times 10^{-2}$ mmol g^{-1}) was comparable with that reported for Al_2O_3 [40, 41], CeO_2 [59], and TiO_2 [60, 61] supported Au systems ($10\text{-}38 \times 10^{-2}$ mmol g^{-1}).

2.3.2 Catalyst Performance

Reaction over supported Au under conditions of excess hydrogen (H_2/LA = 420) generated GVL as sole product at $X \leq 0.75$ (**Figure 2.4(I)**). This response finds agreement with the work of Du *et al*. [62] in batch liquid phase conversion of LA + formic acid (5 bar) over (ZrO_2, TiO_2, SiO_2) supported Au where CO_2 was formed as by-product (from formic acid). We provide here the first reported catalytic data for gas phase continuous flow operation at ambient pressure over Au catalysts. Taking the reaction pathways presented in **Figure 2.1**, GVL generation through the formation of (levulinic and hydroxy levulinic) esters (steps **(I-II)**) is associated with batch liquid operation with alcohol solvents [63]. The LA → GVL composite hydrogenation/dehydration is possible *via* two routes. Reaction through steps **(VI)** and **(VII)** involves hydrogenation of the ketone group at metal sites to form 4-hydroxypentanoic acid (HPA) that undergoes acid-catalysed ring closure (intramolecular esterification) [6]. There is theoretical (DFT) [64, 65] and experimental [65] evidence that LA → HPA hydrogenation (step **(VI)**) is rate-determining. HPA is highly reactive and readily undergoes dehydration to GVL [66]. Alternatively, dehydration of LA (step **(VIII)**) on acid sites generates α-angelica lactone (AGL) that undergoes reduction to GVL (step **(IX)**) [67].

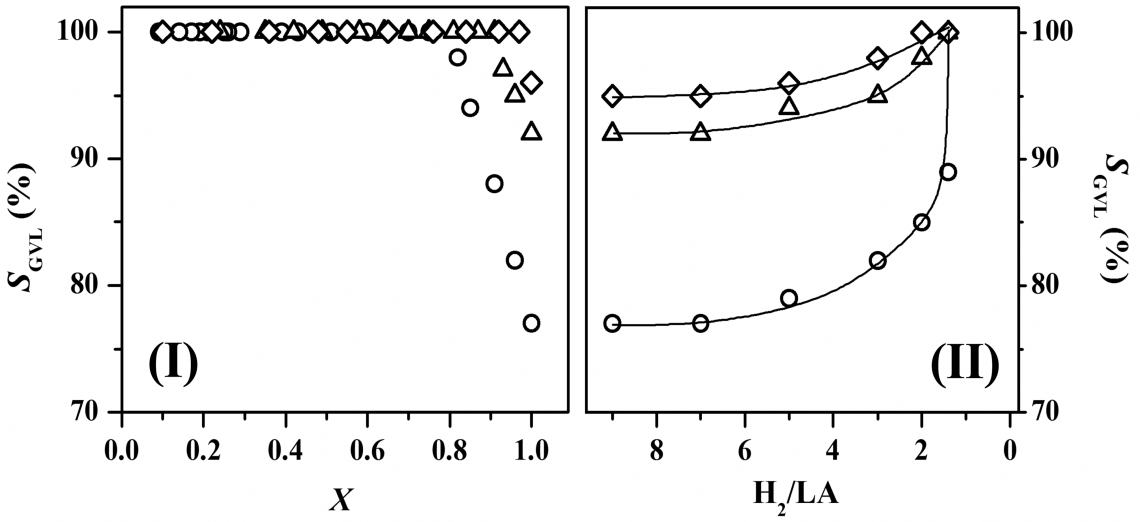

Figure 2. 4: Variation of γ-valerolactone selectivity (S_{GVL}) with (I) levulinic acid (LA) fractional conversion (X) under reaction conditions in excess of hydrogen (H_2/LA = 420) and (II) inlet H_2/LA at full LA conversion (X = 1) over Au/Al_2O_3 (○), Au/CeO_2 (△) and Au/TiO_2 (◇); *Reaction Conditions*: T = 493-573 K, P = 1 atm, $n/F = 5 \times 10^{-4} - 1 \times 10^{-2}$ h.

The HPA or AGL intermediates were not isolated in the product mixture. Conversion of LA to AGL *via* step **(VIII)** is favoured by replacing H_2 with N_2 as gas carrier, circumventing reduction (step **(VI)**). Switching from H_2O to toluene as LA solvent should also favour dehydration to AGL. Reaction (at 573 K) in N_2 using toluene over the three Au catalysts resulted in exclusive LA → AGL at a similar low conversion ($X \leq 0.08$). At the same reaction temperature, catalyst tests using the three systems in H_2 with H_2O promoted LA → GVL at 10-fold higher conversion. Transformation of an aqueous LA feed (in H_2) to GVL must proceed predominantly *via* HPA in a sequential hydrogenation and dehydration (steps **(VI)** and **(VII))**. It is established that acid sites contribute to dehydration [23]. The three Au catalysts exhibit similar surface acidity (see **Figure 2.2(II)** and **Table 2.1**), which did not promote significant LA → AGL but must contribute to HPA → GVL (step **(VII)**) in the sequential conversion of LA. Balla *et al.* [68] and Kumar and co-workers [69] showed that catalytic activity in the gas phase transformation of LA → AGL is dependent on the concentration [68] and type [69] of acid sites.

We have previously established the applicability of pseudo-first order kinetics for hydrogenation over Au under plug-flow conditions where H_2 was maintained in excess [47] according to

$$\ln(1-X)^{-1} = k \times \left(\frac{n}{F}\right) \quad \textbf{(2.3)}$$

where the parameter *n/F* has the physical significance of contact time. The rate constants (*k*) obtained from linear regression of $\ln(1-X)^{-1}$ *vs*. *n/F* (**Figure 2.5**) were fitted to an Arrhenius expression to give an apparent activation energy for LA → GVL of 35 kJ mol^{-1} (see inset to **Figure 2.5** for Au/Al_2O_3). This is within the range (26-54 kJ mol^{-1}) [6] reported for liquid phase reaction over Ru catalysts. The activity of Au/Al_2O_3 was appreciably lower than that of Au on reducible supports (**Table 2.1**). Differences in rate can result from variations in H_2 uptake under reaction conditions [70]. However, the three supported catalysts exhibit an equivalent chemisorption capacity (**Table 2.1**). It is significant that Au/CeO_2 and Au/TiO_2 with similar density of oxygen vacancies (and greater than Au/Al_2O_3) delivered an equivalent catalytic activity. A possible contribution due to LA adsorption/activation at these vacancies should then be considered. Calaza *et al.* [71] have established (by TPD, RAIRS and DFT) carbonyl group activation at oxygen vacancies on CeO_2. To probe this effect we evaluated the catalytic response of physical mixtures of Au/Al_2O_3 with (*non*-reducible) Al_2O_3 and (reducible) TiO_2/CeO_2. Reaction over Au/Al_2O_3+Al_2O_3 and Au/Al_2O_3 delivered the same LA consumption rate (300 $mmol_{GVL}$ g_{metal}^{-1} h^{-1}). In contrast, Au/Al_2O_3+TiO_2 and Au/Al_2O_3+CeO_2 combinations exhibited measurably higher rates (500-600 $mmol_{GVL}$ g_{metal}^{-1} h^{-1}). Oxygen vacancy formation in CeO_2 and TiO_2 as part of the Au/Al_2O_3+TiO_2 and Au/Al_2O_3+CeO_2 mixtures is possible by spillover hydrogen migration across solid/solid grain boundaries [72]. The greater activity of Au/Al_2O_3 with reducible CeO_2 and TiO_2 suggests a direct contribution of these surface defects to catalytic activity. A similar conclusion was reached by Manyar *et al.* [73] and Hu and co-workers [74] in the hydrogenation of carboxylic acids and dimethyl succinate (to γ-butyrolactone) over TiO_2 supported Pt and Mn spinel-supported Cu, respectively.

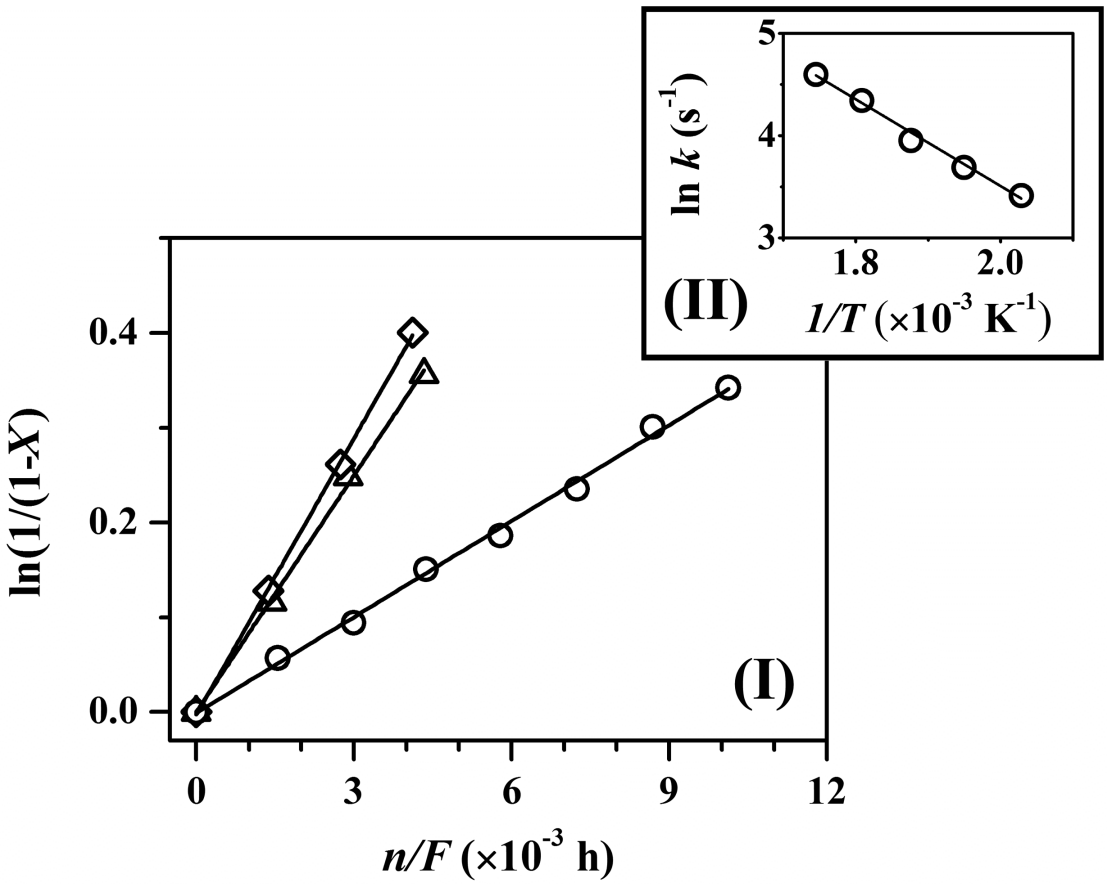

Figure 2. 5: (I) Pseudo-first order kinetic plot for the conversion of levulinic acid (LA) to γ-valerolactone (GVL) over Au/Al_2O_3 (○), Au/CeO_2 (△) and Au/TiO_2 (◇) with (II) Arrhenius plot for reaction over Au/Al_2O_3; *Reaction Conditions*: T = 493-573 K, P = 1 atm, H_2/LA = 420.

At higher LA conversion ($X > 0.75$), GVL selectivity declined (**Figure 2.4(I)**) due to the formation of pentanoic acid. The generation of pentanoic acid can result from HPA hydrogenation-dehydration (step **(IV)** in **Figure 2.1**) or further conversion of GVL (step **(V)**). Kumar *et al*. [69] has shown by combined pyridine adsorption/DRIFTS analysis and kinetic measurements that acid sites promote GVL ring opening to pentanoic acid. Using GVL as reactant under the same reaction conditions, we recorded negligible conversion ($X < 0.03$), suggesting step **(IV)** as the predominant source of pentanoic acid.

Unwanted transformation of HPA to pentanoic acid (*via* step **(IV)** in **Figure 2.1**) requires hydrogen. With a view to maximise GVL formation and limit pentanoic acid

formation we evaluated the catalytic response to modifications in H_2 content in the feed (inlet H_2/LA); the results obtained are presented in **Figure 2.4(II)**. A decrease in H_2/LA served to increase GVL selectivity to reach 100% yield over the three catalysts under stoichiometric conditions. Levulinic acid transformation is typically operated under an excess of pressurised gaseous H_2 in order to maximise product yield [11-13]. Mohan *et al.* [75] studied the effect of H_2/LA molar ratio for reaction over Ni/H-ZSM-5 and reported a maximum 92% GVL yield at H_2/LA = 8. The authors recorded lower conversions at H_2/LA < 8 while formation of pentanoic acid was promoted at H_2/LA > 8. To the best of our knowledge, this is the first report of 100% GVL yield in continuous operation with full hydrogen utilisation. Under these reaction conditions, Pd/Al_2O_3 delivered a higher LA consumption rate than Au/Al_2O_3 (1090 *vs.* 300 $mmol_{GVL}\ g_{metal}^{-1}\ h^{-1}$), that correlates well with the reported higher activity for Pd (*vs.* Au) in hydrogenations [76, 77] but promoted undesired pentanoic acid ($S_{Pentanoic\ acid}$ = 10%). We have recorded 100% yield of GVL with an order of magnitude greater productivity relative to the state-of-the art supported Pd and Ru catalysts [5, 7, 17]. Our results demonstrate that oxide supported Au promotes GVL formation *via* HPA where catalytic activity is sensitive to the redox nature of the oxide carrier.

2.4 Conclusions

In the gas phase continuous catalytic conversion of (aqueous) LA, 100% yield of target GVL was achieved under stoichiometric conditions (H_2/LA = 1) over oxide (Al_2O_3, CeO_2 and TiO_2) supported Au. The formation of GVL results from hydrogenation/dehydration with HPA as reactive intermediate. Oxygen titration following TPR established partial reduction of CeO_2 and TiO_2 where Au on reducible supports delivered a higher GVL production rate (relative to Au/Al_2O_3) that is linked to LA activation at surface oxygen vacancies. Palladium on Al_2O_3 as benchmark exhibited higher LA consumption rates but promoted formation of pentanoic acid. Higher H_2 feed content (H_2/LA >2) generated pentanoic acid over the Au catalysts. Continuous GVL formation at ambient pressure from an aqueous LA feed represents a significant advancement over current pressurised batch liquid operations using organic solvents. We have demonstrated full hydrogen utilisation and an order of magnitude higher GVL

production rate than current state-of-the art supported Pd and Ru catalysts.

2.5 References

[2.1] D.M. Alonso, S.G. Wettstein and J.A. Dumesic, *Gamma-Valerolactone, A Sustainable Platform Molecule Derived from Lignocellulosic Biomass*. Green Chem., 2013. **15**: p. 584-595.

[2.2] B. Girisuta, L.P.B.M. Janssen and H.J. Heeres, *International Conference on Sustainable (Bio)Chemical Process Technology Green Chemicals*. Chem. Eng. Res. Des., 2006. **84**: p. 339-349.

[2.3] R. Weingarten, Y.T. Kim, G.A. Tompsett, A. Fernández, K.S. Han, E.W. Hagaman, Jr.W.C. Conner, J.A. Dumesic and G.W. Huber, *Conversion of Glucose into Levulinic Acid with Solid Metal(IV) Phosphate Catalysts*. J. Catal., 2013. **304**: p. 123-134.

[2.4] A.D. Patel, J.C. Serrano-Ruiz, J.A. Dumesic and R.P Anex, *Techno-economic Analysis of 5-Nonanone Production from Levulinic Acid*. Chem. Eng. J., 2010. **160**: p. 311-321.

[2.5] W.R.H. Wright and R. Palkovits, *Development of Heterogeneous Catalysts for the Conversion of Levulinic Acid to γ-Valerolactone*. Chem. Sus. Chem., 2012. **5**: p. 1657-1667.

[2.6] O.A. Abdelrahman, A. Heyden and J.Q. Bond, *Analysis of Kinetics and Reaction Pathways in the Aqueous-phase Hydrogenation of Levulinic Acid to form γ-Valerolactone over Ru/C*. ACS Catal., 2014. **4**: p. 1171-1181.

[2.7] K. Yan, Y. Yang, J. Chai and Y. Lu, *Catalytic Reactions of Gamma-Valerolactone: A Platform to Fuels and Value-added Chemicals*. Appl. Catal. B: Environ., 2015. **179**: p. 292-304.

[2.8] V. Mohan, V. Venkateshwarlu, C.V. Pramod, B.D. Raju and K.S.R. Rao, *Vapour Phase Hydrocyclisation of Levulinic Acid to γ-Valerolactone over Supported Ni Catalysts*. Catal. Sci. Technol., 2014. **4**: p. 1253-1259.

[2.9] P.P. Upare, J.-M. Lee, D.W. Hwang, S.B. Halligudi, Y.K. Hwang and J.-S. Chang, *Selective Hydrogenation of Levulinic Acid to γ-Valerolactone over Carbon-supported Noble Metal Catalysts*. J. Ind. Eng. Chem., 2011. **17**: p. 287-

292.

[2.10] W. Luo, U. Deka, A.M. Beale, E.R.H. Eck, P.C.A. Bruijnincx and B.M. Weckhuysen, *Ruthenium-catalyzed Hydrogenation of Levulinic Acid: Influence of the Support and Solvent on Catalyst Selectivity and Stability*. J. Catal., 2013. **301**: p. 175-186.

[2.11] H. Mehdi, V. Fábos, R. Tuba, A. Bodor, L.T. Mika and I.T. Horváth, *Integration of Homogeneous and Heterogeneous Catalytic Processes for a Multi-step Conversion of Biomass: From Sucrose to Levulinic Acid, γ-Valerolactone, 1,4-Pentanediol, 2-Methyl-tetrahydrofuran, and Alkanes*. Top. Catal., 2008. **48**: p. 49-54.

[2.12] K. Yan, T. Lafleur, G. Wu, J. Liao, C. Ceng and X. Xie, *Highly Selective Production of Value-added γ-Valerolactone from Biomass-derived Levulinic Acid using the Robust Pd Nanoparticles*. Appl. Catal. A: Gen., 2013. **468**: p. 52-58.

[2.13] Z.-P. Yan, L. Lin and S. Liu, *Synthesis of γ-Valerolactone by Hydrogenation of Biomass-derived Levulinic Acid over Ru/C Catalyst*. Energy Fuels, 2009. **23**: p. 3853-3858.

[2.14] U. Omoruyi, S. Page, J. Hallett and P.W. Miller, *Homogeneous Catalyzed Reactions of Levulinic Acid: To γ-Valerolactone and Beyond*. Chem. Sus. Chem., 2016. **9**: p. 2037-2047.

[2.15] I.M. Mándity, S.B. Ötvös and F. Fülöp, *Strategic Application of Residence-time Control in Continuous-flow Reactors*. ChemistryOpen, 2015. **4**: p. 212-223.

[2.16] Y. Hao, M. Li, F. Cárdenas-Lizana and M.A. Keane, *Selective Production of Benzylamine via Gas Phase Hydrogenation of Benzonitrile over Supported Pd Catalysts*. Catal. Lett., 2016. **146**: p. 109-116.

[2.17] I. Delidovich, P.J.C. Hausoul, L. Deng, R. Pfützenreuter, M. Rose and R. Palkovits, *Alternative Monomers Based on Lignocellulose and Their Use for Polymer Production*. Chem. Rev., 2016. **116**: p. 1540-1599.

[2.18] S.D. Richardson and S.Y. Kimura, *Water Analysis: Emerging Contaminants and Current Issues*. Anal. Chem., 2016 **88**: p. 546-582.

[2.19] M. Hara, K. Nakajima and K. Kamata, *Recent Progress in the Development of Solid Catalysts for Biomass Conversion into High Value-added Chemicals*. Sci. Technol. Adv. Mater., 2015. **16**: p. 1-22.

[2.20] J. Ohyama, A. Esaki, Y. Yamamoto, S. Arai and A. Satsuma, *Selective Hydrogenation of 2-Hydroxymethyl-5-furfural to 2,5-Bis(hydroxymethyl)furan over Gold Sub-nano Clusters*. RSC Adv., 2013 **3**: p. 1033-1036.

[2.21] Z. Wei, Y. Li, D. Thushara, Y. Liu and Q. Ren, *Novel Dehydration of Carbohydrates to 5-Hydroxymethylfurfural Catalyzed by Ir and Au Chlorides in Ionic Liquids*. J. Taiwan Inst. Chem. Eng., 2011. **42**: p. 363-370.

[2.22] G. Budroni and A. Corma, *Gold and Gold-platinum as Active and Selective Catalyst for Biomass Conversion: Synthesis of γ-Butyrolactone and One-pot Synthesis of Pyrrolidone.* J. Catal., 2008. **257**: p. 403-408.

[2.23] R. Weingarten, G.A. Tompsett, Jr.W.C. Conner and G.W. Huber, *Design of Solid Acid Catalysts for Aqueous-phase Dehydration of Carbohydrates: The Role of Lewis and Brønsted Acid Sites*. J. Catal., 2011. **279**: p. 174-182.

[2.24] M.V. Ganduglia-Pirovano, A. Hofmann and J. Sauer, *Oxygen Vacancies in Transition Metal and Rare Earth Oxides: Current State of Understanding and Remaining Challenges*. Surf. Sci. Rep., 2007. **62**: p. 219-270.

[2.25] D.R. Mullins, *The Surface Chemistry of Cerium Oxide*. Surf. Sci. Rep., 2015. **70**: p. 42-85.

[2.26] R.S. Smith, Z. Li, L. Chen, Z. Dohnálek and B.D. Kay, *Adsorption, Desorption, and Displacement Kinetics of H_2O and CO_2 on $TiO_2(110)$*. J. Phys. Chem. B, 2014. **118**: p. 8054-8061.

[2.27] E. Farfan-Arribas and R.J. Madix, *Role of Defects in the Adsorption of Aliphatic Alcohols on the $TiO_2(110)$ Surface*. J. Phys. Chem. B, 2002. **106**: p. 10680-10692.

[2.28] J. Zhou and D.R. Mullins, *Adsorption and Reaction of Formaldehyde on Thin-film Cerium Oxide*. Surf. Sci., 2006. **600**: p. 1540-1546.

[2.29] A. Sepúlveda-Escribano, F. Coloma and F. Rodríguez-Reinoso, *Promoting Effect of Ceria on the Gas Phase Hydrogenation of Crotonaldehyde over Platinum*

Catalysts. J. Catal., 1998. **178**: p. 649-657.

[2.30] C. Milone, R. Ingoglia, L. Schipilliti, C. Crisafulli, G. Neri and S. Galvagno, *Selective Hydrogenation of α,β-Unsaturated Ketone to α,β-Unsaturated Alcohol on Gold-supported Iron Oxide Catalysts: Role of the Support*. J. Catal., 2005. **236**: p. 80-90.

[2.31] L.R. Baker, G. Kennedy, M. Spronsen, A. Hervier, X. Cai, S. Chen, L.-W. Wang and G.A. Somorjai, *Furfuraldehyde Hydrogenation on Titanium Oxide-supported Platinum Nanoparticles Studied by Sum Frequency Generation Vibrational Spectroscopy: Acid–base Catalysis Explains the Molecular Origin of Strong Metal–support Interactions*. J. Am. Chem. Soc., 2012. **134**: p. 14208-14216.

[2.32] J. Paier, C. Penschke and J. Sauer, *Oxygen Defects and Surface Chemistry of Ceria: Quantum Chemical Studies Compared to Experiment*. Chem. Rev., 2013. **113**: p. 3949-3985.

[2.33] B. Bachiller-Baeza, I. Rodríguez-Ramos and A. Guerrero-Ruiz, *Influence of Mg and Ce Addition to Ruthenium based Catalysts used in the Selective Hydrogenation of α,β-Unsaturated Aldehydes*. Appl. Catal. A: Gen., 2001. **205**: p. 227-237.

[2.34] M. Khoudiakov, M.C. Gupta and S. Deevi, *Au/Fe_2O_3 Nanocatalysts for CO Oxidation: A Comparative Study of Deposition–precipitation and Coprecipitation Techniques*. Appl. Catal. A: Gen., 2005. **291**: p. 151-161.

[2.35] F. Lónyi and J. Valyon, *On the Interpretation of the NH_3-TPD Patterns of H-ZSM-5 and H-Mordenite*. Micropor. Mesopor. Mater., 2001. **47**: p. 293-301.

[2.36] S. Salasc, V. Perrichon, M. Primet, M. Chevrier and N. Mouaddib-Moral, *Oxygen Titration of Spill-over Hydrogen in Ceria and Ceria–alumina Supported Platinum–rhodium Catalysts: Application to the Determination of the Ceria Surface in Contact with Metal*. J. Catal., 2000. **189**: p. 401-409.

[2.37] G.C. Bond, C. Louis and D.T. Thompson, *Catalysis by Gold*, Imperial College Press, London, 2006.

[2.38] F. Cárdenas-Lizana, X. Wang, D. Lamey, M. Li, M.A. Keane and L. Kiwi-

Minsker, *An Examination of Catalyst Deactivation in Nitroarene Hydrogenation over Supported Gold*. Chem. Eng. J., 2014. **255**: p. 695-704.

[2.39] F. Cárdenas-Lizana, S. Gómez-Quero, M.A. Keane, *Clean Production of Chloroanilines by Selective Gas Phase Hydrogenation Over Supported Ni Catalysts*. Appl. Catal. A: Gen., 2008. **334**: p. 199-206.

[2.40] S.Y. Liu and S.M. Yang, *Complete Oxidation of 2-Propanol over Gold-based Catalysts Supported on Metal Oxides*. Appl. Catal. A: Gen., 2008. **334**: p. 92-99.

[2.41] Y. Zhang, Q. Xiao, Y. Bao, Y. Zhang, S. Bottle, S. Sarina, B. Zhaorigetu and H. Zhu, *Direct Photocatalytic Conversion of Aldehydes to Esters Using Supported Gold Nanoparticles under Visible Light Irradiation at Room Temperature*. J. Phys. Chem. C, 2014. **118**: p. 19062-19069.

[2.42] Y. Hao, X. Wang, N. Perret, F. Cárdenas-Lizana and M.A. Keane, *Support Effects in the Gas Phase Hydrogenation of Butyronitrile over Palladium*. Catal. Struct. React., 2015. **1**: p. 4-10.

[2.43] C.K. Costello, J. Guzman, J.H. Yang, Y.M. Wang, M.C. Kung, B.C. Gates and H.H. Kung, *Activation of Au/γ-Al_2O_3 Catalysts for CO Oxidation: Characterization by X-ray Absorption Near Edge Structure and Temperature Programmed Reduction*. J. Phys. Chem. B, 2004. **108**: p. 12529-12536.

[2.44] L. Delannoy, N. Weiher, N. Tsapatsaris, A.M. Beesley, L. Nchari, S.L.M. Schroeder and C. Louis, *Reducibility of Supported Gold (III) Precursors: Influence of the Metal Oxide Support and Consequences for CO Oxidation Activity*. Top. Catal., 2007. **44**: p. 263-273.

[2.45] M. Ousmane, L.F. Liotta, D. Carlo, G. Pantaleo, A.M. Venezia, G. Deganello, L. Retailleau, A. Boreave and A. Giroir-Fendler, *Supported Au Catalysts for Low-temperature Abatement of Propene and Toluene, as Model VOCs: Support Effect*. Appl. Catal. B: Environ., 2011. **101**: p. 629-637.

[2.46] B. Hammer and J.K. Nørskov, *Why Gold is the Noblest of All the Metals*. Nature, 1995. **376**: p. 238-240.

[2.47] F. Cárdenas-Lizana and M.A. Keane, *The Development of Gold Catalysts for Use in Hydrogenation Reactions*. J. Mater. Sci., 2013. **48**: p. 543-564.

[2.48] E. Bus, J.T. Miller and J.A. Bokhoven, *Hydrogen Chemisorption on Al_2O_3-supported Gold Catalysts*. J. Phys. Chem. B, 2005. **109**: p. 14581-14587.

[2.49] N.A. Joy, M.I. Nandasiri, P.H. Rogers, W. Jiang, T. Varga, S.V.N.T. Kuchibhatla, S. Thevuthasan and M.A. Carpenter, *Selective Plasmonic Gas Sensing: H_2, NO_2, and CO Spectral Discrimination by a Single Au-CeO_2 Nanocomposite Film*. Anal. Chem., 2012. **84**: p. 5025-5034.

[2.50] T.-Y. Ma, J.-L. Cao, G.-S. Shao, X.-J. Zhang and Z.-Y. Yuan, *Hierarchically Structured Squama-like Cerium-Doped Titania: Synthesis, Photoactivity, and Catalytic CO Oxidation*. J. Phys. Chem. C, 2009. **113**: p. 16658-16667.

[2.51] R.L. Oliveira, I.G. Bitencourt and F.B. Passos, *Partial Oxidation of Methane to Syngas on Rh/Al_2O_3 and Rh/Ce-ZrO_2 Catalysts*. J. Braz. Chem. Soc., 2013. **24**: p. 68-75.

[2.52] J. Radnik, C. Mohr and P. Claus, *On the Origin of Binding Energy Shifts of Core Levels of Supported Gold Nanoparticles and Dependence of Pretreatment and Material Synthesis*. Phys. Chem. Chem. Phys., 2003. **5**: p. 172-177.

[2.53] C.T. Campbell and C.H.F. Peden, *Oxygen Vacancies and Catalysis on Ceria Surfaces*. Science, 2005. **309**: p. 713-714.

[2.54] I. Prymak, V.N. Kalevaru, S. Wohlrab and A. Martin, *Continuous Synthesis of Diethyl Carbonate from Ethanol and CO_2 over Ce-Zr-O Catalysts*. Catal. Sci. Technol., 2015. **5**: p. 2322-2331.

[2.55] E. Farfan-Arribas and R.J. Madix, *Characterization of the Acid−Base Properties of the TiO_2(110) Surface by Adsorption of Amines*. J. Phys. Chem. B, 2003. **107**: p. 3225-3233.

[2.56] P.J. Chupas and C.P. Grey, *Surface Modification of Fluorinated Aluminas: Application of Solid State NMR Spectroscopy to the Study of Acidity and Surface Structure*. J. Catal., 2004. **224**: p. 69-79.

[2.57] M.A. Jaoude, K. Polychronopoulou, S.J. Hinder, M.S. Katsiotis, M.A. Baker, Y.E. Greish and S.M. Alhassan, *Synthesis and Properties of 1D Sm-doped CeO_2 Composite Nanofibers Fabricated using a Coupled Electrospinning and Sol–gel Methodology*. Ceram. Int., 2016. **42**: p. 10734-10744.

[2.58] C. Morterra and G. Magnacca, *A Case Study: Surface Chemistry and Surface Structure of Catalytic Aluminas, As Studied by Vibrational Spectroscopy of Adsorbed Species*. Catal. Today, 1996. **27**: p. 497-532.

[2.59] C. Santra, M. Pramanik, K.K. Bando, S. Maity and B. Chowdhury, *Gold Nanoparticles on Mesoporous Cerium-Tin Mixed Oxide for Aerobic Oxidation of Benzyl Alcohol*. J. Mol. Catal. A: Chem., 2016. **418–419**: p. 41-53.

[2.60] P.N. Amaniampong, K. Li, X. Jia, B. Wang, A. Borgna and Y. Yang, *Titania-Supported Gold Nanoparticles as Efficient Catalysts for the Oxidation of Cellobiose to Organic Acids in Aqueous Medium*. Chem. Cat. Chem., 2014. **6**: p. 2105-2114.

[2.61] M. Yang, Y. Men, S. Li and G. Chen, *Enhancement of Catalytic Activity over TiO_2-modified Al_2O_3 and $ZnO–Cr_2O_3$ Composite Catalyst for Hydrogen Production via Dimethyl Ether Steam Reforming*. Appl. Catal. A: Gen., 2012. **433-434**: p. 26-34.

[2.62] X.-L. Du, L. He, S. Zhao, Y.-M. Liu, Y. Cao,H.-Y. He and K.-N. Fan, *Hydrogen-independent Reductive Transformation of Carbohydrate Biomass into γ-Valerolactone and Pyrrolidone Derivatives with Supported Gold Catalysts*. Angew. Chem.-Int. Edit., 2011. **50**: p. 7815-7819.

[2.63] H. Heeres, R. Handana, D. Chunai, C.B. Rasrendra, B. Girisuta and H.J. Heeres, *Combined Dehydration/(transfer)-hydrogenation of C6-sugars (D-glucose and D-fructose) to γ-valerolactone using Ruthenium catalysts.* Green Chem., 2009. **11**: p.1247-1255.

[2.64] H. Gao and J. Chen, *Hydrogenation of Biomass-derived Levulinic Acid to γ-Valerolactone Catalyzed by PNP-Ir Pincer Complexes: A Computational Study*. J. Organomet. Chem., 2015. **797**: p. 165-170.

[2.65] C. Michel, J. Zaffran, A.M. Ruppert, J. Matras-Michalska, M. Jędrzejczyk, J. Grams and P. Sautet, *Role of Water in Metal Catalyst Performance for Ketone Hydrogenation: A Joint Experimental and Theoretical Study on Levulinic Acid Conversion into γ-Valerolactone*. Chem. Commun., 2014. **50**: p. 12450-12453.

[2.66] A.B. Jain and P.D. Vaidya, *Kinetics of the Ruthenium-catalyzed Hydrogenation*

of Levulinic Acid to γ-Valerolactone in Aqueous Solutions. Can. J. Chem. Eng., 2016. **94**: p. 2364-2372.

[2.67] V.V. Kumar, G. Naresh, M. Sudhakar, C. Anjaneyulu, S.K. Bhargava, J. Tardio, V.K. Reddy, A.H. Padmasri and A. Venugopal, *An Investigation on the Influence of Support Type for Ni Catalysed Vapour Phase Hydrogenation of Aqueous Levulinic Acid to γ-Valerolactone*. RSC Adv., 2016. **6**: p. 9872-9879.

[2.68] P. Balla, V. Perupogu, P.K. Vanama and V.R.C. Komandur, *Hydrogenation of Biomass-derived Levulinic Acid to γ-Valerolactone over Copper Catalysts Supported on ZrO_2*. J. Chem. Technol. Biotechnol., 2016. **91**: p. 769-776.

[2.69] V.V. Kumar, G. Naresh, M. Sudhakar, J. Tardio, S.K. Bhargava and A. Venugopal, *Role of Brønsted and Lewis Acid Sites on Ni/TiO_2 Catalyst for Vapour Phase Hydrogenation of Levulinic Acid: Kinetic and Mechanistic Study*. Appl. Catal. A: Gen., 2015. **505**: p. 217-223.

[2.70] M. Li, X. Wang, Y. Hao, F. Cárdenas-Lizana and M.A. Keane, *Effect of Support Redox Character on Catalytic Performance in the Gas Phase Hydrogenation of Benzaldehyde and Nitrobenzene over Supported Gold*. Catal. Today, 2017. **279**: p. 19-28.

[2.71] F.C. Calaza, Y. Xu, D.R. Mullins and S.H. Overbury, *Oxygen Vacancy-assisted Coupling and Enolization of Acetaldehyde on CeO_2(111)*. J. Am. Chem. Soc., 2012. **134**: p. 18034-18045.

[2.72] F. Röbner, *Chapter 5. Elementary Steps and Mechanisms. Section 5.3.2 Spillover Effects* in Handbook of Heterogeneous Catalysis, ed. by G.H.K. Ertl, F. Schütz, J. Weitkamp. Wiley-VCH, Weinheim, 2008, p. 1051-1188.

[2.73] H.G. Manyar, C. Paun, R. Pilus, D.W. Rooney, J.M. Thompson and C. Hardacre, *Highly Selective and Efficient Hydrogenation of Carboxylic Acids to Alcohols using Titania Supported Pt Catalysts*. Chem. Commun., 2010. **46**: p. 6279-6281.

[2.74] Q. Hu, L. Yang, G. Fan and F. Li, *Hydrogenation of Biomass-derived Compounds Containing a Carbonyl Group over a Copper-based Nanocatalyst: Insight into the Origin and Influence of Surface Oxygen Vacancies*. J. Catal.,

2016. **340**: p. 184-195.

[2.75] V. Mohan, C. Raghavendra, C.V. Pramod, B.D. Raju and K.S.R. Rao, *Ni/H-ZSM-5 as a Promising Catalyst for Vapour Phase Hydrogenation of Levulinic Acid at Atmospheric Pressure*. RSC Adv., 2014. **4**: p. 9660-9668.

[2.76] F. Cárdenas-Lizana, S. Gómez-Quero and M.A. Keane, *Ultra-selective Gas Phase Catalytic Hydrogenation of Aromatic Nitro Compounds over Au/Al_2O_3*. Catal. Commun., 2008. **9**: p. 475-481.

[2.77] X. Wang, Y. Hao and M.A. Keane, *Selective Gas Phase Hydrogenation of p-Nitrobenzonitrile to p-Aminobenzonitrile over Zirconia Supported Gold*. Appl. Catal. A: Gen., 2016. **510**: p. 171-179.

Chapter 3

Catalytic Single-pot Methyl-N-Phenyl Carbamate Production From CO_2, Methanol and Nitrobenzene. Influence of the ceria redox properties

In the previous chapter, support redox character was established as a critical catalyst feature that determined performance in the transformation of levulinic acid. That work is extended in this chapter, where the role of Ce^{3+}/Ce^{4+} ratio for as prepared/received and calcined CeO_2 and Pd/CeO_2 catalysts has been examined with respect to single-pot methyl-N-phenyl carbamate (MPC) production from CO_2, methanol and nitrobenzene (NB).

3.1 Introduction

The utilisation of carbon dioxide in the production of fine chemicals is receiving significant attention [1, 2]. Only *ca.* 2×10^8 tonnes $year^{-1}$ of CO_2 emissions is utilised by the chemical industries [3] due to high energy requirement for C-O bond activation [4]. CO_2 has been converted to a range of products including formic acid [5], methanol [6], carbonates [7, 8], carbamates [9], urethane intermediates [10] and carboxylated allyl derivatives [11]. The conversion to carbamates and carbonates is one of the most promising alternatives because of their ability to form polyurethanes and polycarbonates [12-14], which are extensively produced in industry (7.5×10^6 tonnes $year^{-1}$ in China alone in 2011 [15]). Commercial synthesis of carbamates involves reaction of amines with toxic phosgene [14, 16]. Methyl-N-Phenyl carbamate (MPC) is a simplest carbamate and valuable intermediate for the synthesis of polyurethane, pesticides and herbicides [16]. The main non-phosgene methods for synthesising carbamates include oxidative carbonylation of an amines [17, 18], reductive carbonylation of nitroarenes [19, 20] and methoxycarboxylation of an amines [21]. However, many drawbacks (*i.e.* hazardous reactants, harsh operating conditions, high cost, etc. [22]) associated with the

above routes have a negative impact on carbamate production. Among these methods, the methoxycarboxylation of an amine uses carbonate as a reactant, which could be potentially synthesised directly from CO_2 [7, 8]. This will promote CO_2 utilization and provide a cleaner and safer route for carbamate synthesis as water is the only reaction by-product. There have been a few attempts to synthesise carbamates directly from CO_2 [23-25], however due to thermodynamic limitations these reactions were performed under high CO_2 pressures (25-300 atm) and an activity for the formation of target carbamates was below 60%. In order to optimise the production of carbamates in a single-pot, a simplified scheme of reaction pathways involved was considered and is shown in **Figure 3.1**, where dimethyl carbonate (DMC), nitrobenzene (NB), aniline (AN) and MPC were selected as a simplest model molecules. Initially, carboxylation of methanol results in the formation of DMC (**step I**) while the hydrogenation of NB results in the formation of AN (**step II**). Then AN together with DMC undergoes the condensation reaction (**step III**) to form MPC. It has been shown that the step II can be easily performed in the presence of transition metals (i.e. Pd [26], Cu [27], etc.) and step III requires only weak Lewis acid (LWA) sites on the surface of a catalyst [28]. However, the step I appears to be determining due to difficulties associated with CO_2 activation [29] and, therefore, its optimisation is critical for the single-pot carbamate production.

Several homogeneous [30, 31] and heterogeneous [32, 33] catalysts have been employed for the transformation of carbon dioxide to DMC. Among homogeneous ones, Sn and Nb complexes received more attention, however the yield of DMC remains low (≤61%). This was attributed to the conversion of the catalysts into oligomers during reaction that reduces their activity. Heterogeneous catalysts such as CeO_2, ZrO_2 or TiO_2 have also been used but since this reaction is thermodynamically limited [29], most of the work carried out at elevated pressures (PCO_2 = 20 – 300 atm) [29-33] in order to shift the equilibrium towards DMC formation.

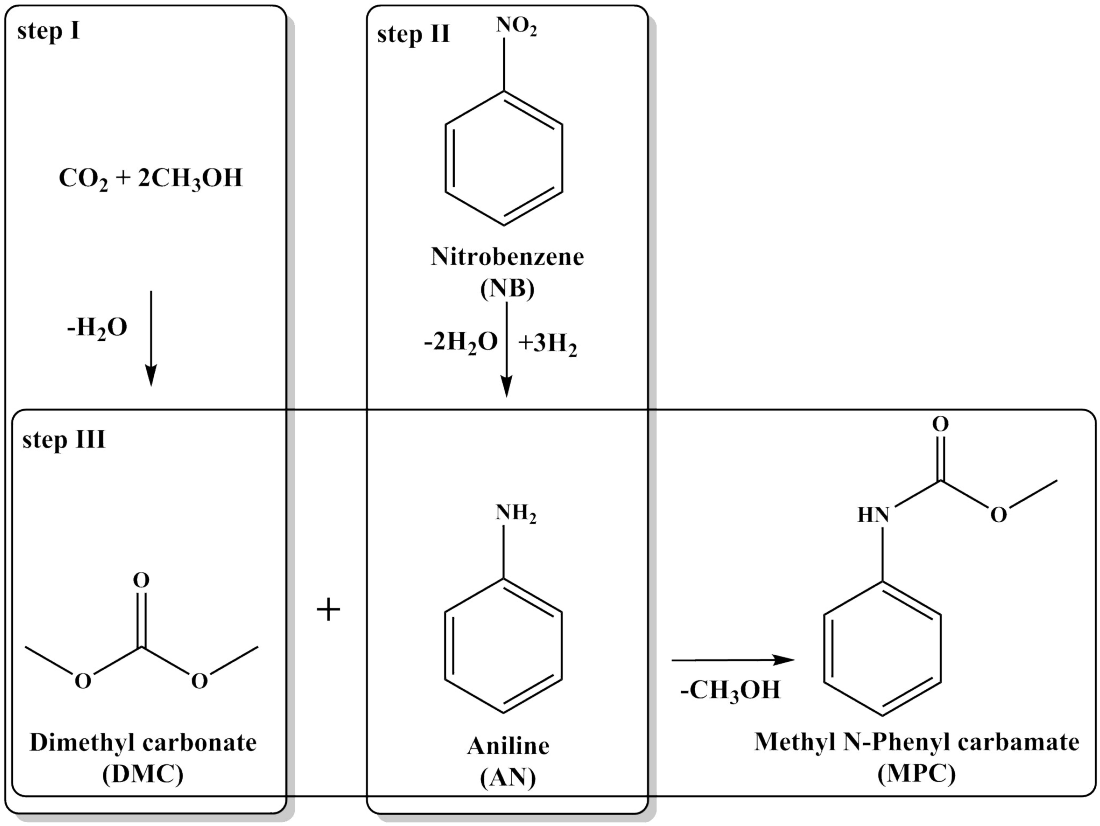

Figure 3. 1: Simplified scheme of reaction pathways involved in the production of methyl N-phenyl carbamate (MPC).

It worth noting, that only a few studies managed to overcome reaction limitations by using a dehydrating agents which help to remove co-produced water from the catalyst surface [34-36]. Honda *et al.* [36] improved the yield (from 0.02 to 1.8 mmol at T = 423 K) of diethyl carbonate (DEC) by using acetonitrile as a dehydrating agent, under low CO_2 pressure (5 atm) and over CeO_2 catalyst. It has been also shown that total acidity and basicity of the catalyst [33, 37, 38] determine activation of CO_2 and methanol, however the type of acid/base sites (Lewis or Brønsted) in DMC production is still not considered. CeO_2 has received much attention because of it redox/oxidation properties, high oxygen mobility and ability to switch between oxidation states (Ce^{3+}/Ce^{4+}) [37]. The modification of Ce^{3+}/Ce^{4+} ratio on the surface of CeO_2 can alter the acid-base configuration [37] and as a result can improve catalytic performance for carbonate production from CO_2. Leino *et al*. [34], studied the effect of CeO_2 preparation variables, where an increase in calcination temperature has been

shown to decrease carbonate production rate ascribed to decrease in specific surface area (SSA). Increase activity was recorded over CeO_2 with greater SSA (up to 2 mmol at T = 453 K and P = 90 atm). Yoshida *et al.* [37] showed the dependence of catalytic activity towards DMC formation to SSA of CeO_2 and suggested that rate is nearly proportional to SSA and the active site of the reaction is on (111) crystal surface of CeO_2. In terms of the redox properties of cerium oxide, it has been shown that the surface modification produced by methanol adsorption (during DMC formation) caused $Ce^{4+} \rightarrow Ce^{3+}$ reduction and catalyst deactivation [39, 40]. However, the role of Ce^{3+}/Ce^{4+} ratio of CeO_2 (before the reaction) on the catalytic activity for the carbonate production has not been considered.

In this study, we demonstrate and optimise the alternative route for MPC production *via* DMC and directly from CO_2. We establish the link between the acid-base properties and Ce^{3+}/Ce^{4+} ratio of CeO_2 and investigate their effect (along with SSA) on catalytic activity for DMC formation. We consider the limitations due to water formation and examine the reaction in gas phase under continuous operation mode and at ambient pressure.

3.2 Experimental

3.2.1 Catalyst Preparation and Pretreatment

A commercial CeO_2 support (CeO_2-comm) was purchased from Sigma Aldrich and used as received. The preparation technique of this commercial support has been described by Hanawa *et al.* [41] and results in the ultrafine particles. A laboratory synthesised CeO_2 sample (CeO_2) was prepared by precipitation at room temperature following a procedure described elsewhere [42]. Briefly, ammonium hydroxide (30 cm^3 h^{-1}, 28-30% NH_3 basis, Sigma Aldrich) was added using a microprocessor controlled infusion pump (Model 100 kd Scientific) at a fixed calibrated flow rate into well stirred (400 rpm) aqueous solution of $Ce(NO_3)_3 \times 6H_2O$ (1 M; 70 cm^3, 99%, Sigma Aldrich) until pH reached 11. This pH is far above the isoelectric point of CeO_2 (*ca.* 6.8) and facilitates cation (Ce^{3+}) deposition from the solution. The synthesis time was set 60 h in order to achieve high porosity of the material after nucleation and, therefore, high

surface area [35]. The resultant precipitate was filtered, washed with deionised water until the pH value reached *ca.* 7 and dried in He (45 cm^3 min^{-1}) at 373 K (2 K min^{-1}) for 5 h. A 4.2% w/w Pd/CeO_2 catalyst was prepared by deposition-precipitation on CeO_2-comm. An aqueous solution of sodium carbonate (>99%, anhydrous, Sigma Aldrich), used as basification agent, was added (2 M, 50 cm^3) dropwise to an aqueous solution of $Pd(NO_3)_2$ (2×10^{-5} M; 300 cm^3, Sigma Aldrich) containing the CeO_2 support (10 g). The suspension was stirred and pH progressively increased to reach *ca.* 10 with precipitation of $Pd(OH)_2$ [43]. The resultant solid was separated by centrifugation, washed with deionised water until the pH reached *ca.* 7 and dried in He (45 cm^3 min^{-1}) at 373 K (2 K min^{-1}) for 5 h.

Prior to use, the catalysts were sieved to 75 μm average particle diameter ATM fine test sieves and activated (in H_2)/calcined (in O_2) at 2 K min^{-1} to 573–873 K. The activated samples were passivated in 1% v/v O_2/He at room temperature for *ex situ* characterisation.

3.2.2 Catalyst Characterisation

The Pd content was measured by atomic absorption spectroscopy (Shimadzu AA-6650 spectrometer with an air-acetylene flame) from the diluted extract in aqua regia (25% v/v HNO_3/HCl). SSA, temperature programmed reduction (TPR), O_2 chemisorption and carbon dioxide temperature programmed desorption (CO_2-TPD) measurements were recorded using the commercial CHEM-BET 3000 (Quantachrome Instruments) unit equipped with a thermal conductivity detector (TCD) for continuous monitoring of gas composition and the TPR Win™ software for data acquisition/manipulation. Samples (0.05-0.1 g) were loaded into a U-shaped Quartz cell (3.76 mm i.d.), outgassed for 30 min (at room temperature) and the total SSA recorded in a 30% v/v N_2/He flow with undiluted N_2 (BOC, 99.9%) as internal standard. Two cycles of N_2 adsorption-desorption were employed using the standard single point BET method. CeO_2 was subjected to CO_2 chemisorption by continuous flow (100 cm^3 min^{-1}, 298 K, 1 atm, BOC, 99.99%). CO_2-TPD in N_2 (65 cm^3 min^{-1}) was conducted at 30 K min^{-1} to 900 K with a final isothermal hold until the signal returned to baseline. SSA and CO_2 release values were reproducible to within ±7% and the values quoted

represent the mean. TPR analysis was conducted in 17 cm^3 min^{-1} (Brooks mass flow controller) 5% v/v H_2/N_2 at 2 K min^{-1} to 573 K, following the reduction procedure established previously [44]. The sample was maintained at the final isothermal hold in a flow of H_2/N_2 until the signal returned to baseline, swept with a 65 cm^3 min^{-1} flow of N_2 for 1.5 h and cooled to room temperature. Oxygen chemisorption was performed to assess the extent of support reduction [45] where the samples were swept with 65 cm^3 min^{-1} He for 1.5 h post-TPR, cooled to 493 K and subjected to O_2 pulse (10 μL) titration.

Powder X-ray diffractograms were recorded on a Bruker/Siemens D500 incident X-ray diffractometer using Cu Kα radiation. The samples were scanned (0.02^o $step^{-1}$) over the range $5^o \leq 2\theta \leq 85^o$. The diffractograms were identified using the JCPDS-ICDD reference standards, *i.e.* CeO_2 (43-1002). Ceria crystallite mean size was estimated from the full width at half maximum (FWHM) and Debye-Scherrer's equation:

$$D = \frac{0.89 \times \lambda}{B \times \cos\theta} \qquad \textbf{(3.1)}$$

where 0.89 is the shape factor, λ is the X-ray wavelength, B is the line broadening at FWHM (in radians) of CeO_2 (111) plane and θ is the Bragg angle. XPS spectra were collected on an Axis Ultra instrument (Kratos Analytical) x-ray photoelectron spectrometer under ultra-high vacuum condition (< 10^{-8} Torr) using an Al Kα (hν =1486.6 eV) x-ray source. The binding energies (BE) were calibrated with respect to the C-C/C-H components of the C 1s peak (BE = 284.7 eV). Spectra processing applied the Casa XPS software package.

3.2.3 Catalytic System

DMC (≥99% w/w), MeOH (99.8% w/w), MPC (97% w/w), AN (≥99.5% w/w), NB (≥99% w/w) and acetonitrile (99.8% w/w) were supplied by Sigma-Aldrich and used as received. All the gases (H_2, N_2, O_2, CO_2 and He) were of ultra high purity (>99.99%, BOC).

3.2.3.1 Carboxylation of Methanol

3.2.3.1.1 Liquid Phase Operation

Liquid phase carboxylation of methanol (T = 423 K; P_{CO_2} = 5 atm) was conducted in a commercial batch stirred stainless steel reactor (100 cm^3 autoclave, Parr reactor) equipped with a pressure controlled CO_2/N_2 supply system. The temperature was maintained at 423 ±1 K by a programmed temperature controller (Parr 4848). At the beginning of each run, the mixture of methanol (8 cm^3), dehydrating agent (acetonitrile, 31 cm^3) and catalyst was introduced to the reactor, sealed and flushed 3 times with N_2 to release the remaining air. The system was then heated to the reaction temperature, pressurised with CO_2 and the stirring was engaged at *ca.* 800 rpm (time t = 0 for reaction). In blank tests, reaction in the absence of catalyst did not result in any measurable conversion. Aliquots (1 cm^3) for analysis were collected *via* a gastight syringe with in-line filters. The catalytic activity was quantified in terms of fractional MeOH conversion (X_{MeOH})

$$X_{MeOH} = \frac{2 \times C_{DMC}}{C_{MeOH,0}} \qquad \textbf{(3.2)}$$

where the subscript "0" refers to initial concentration. The initial rate of DMC production was determined from a linear regression of DMC concentration profiles at $X_{MeOH} < 0.2$ [46].

3.2.3.1.2 Gas Phase Operation

Gas phase carboxylation of methanol (T = 523 – 723 K; P = 1 atm) was carried out in a fixed bed vertical continuous plug-flow glass reactor (*i.d.* = 12 mm). Methanol was vaporised, mixed with CO_2 over a layer of borosilicate glass balls (2 mm diameter) and reached the reaction temperature before contacting the catalyst bed. Reaction temperature was continuously monitored by a thermocouple inserted in a thermowell within the catalyst bed. Pure MeOH was delivered to the reactor *via* a glass/teflon air-tight syringe and a teflon line at a fixed calibrated flow rate using a microprocessor controlled infusion pump (Model 100, KD Scientific). A co-current flow of MeOH and

CO_2 was maintained at $GHSV = 1\times 10^4 - 2 \times 10^4$ h^{-1} with an inlet MeOH molar flow (F_{MeOH}) of $1 \times 10^{-2} - 3 \times 10^{-2}$ mol h^{-1}. The rate of DMC production was insensitive to variation in contact time (τ) from 0.2 to 0.4 s, indicative of minimal external mass and/or heat transport contributions. Passage of MeOH in a stream of CO_2 through the empty reactor did not result in any detectable conversion. The fractional conversion of MeOH was defined as

$$X_{\mathrm{MeOH}} = \frac{2 \times C_{\mathrm{DMC,out}}}{C_{\mathrm{MeOH,in}}} \qquad \textbf{(3.3)}$$

where the subscripts "in" and "out" refer to the inlet and outlet streams.

3.2.3.2 Single-pot Carbamate Production

Gas Phase production of MPC (T = 723 K; P = 1 atm) was carried out in a fixed bed vertical continuous plug-flow glass reactor (i.d. = 12 mm). A mixture of MeOH and NB (MeOH:NB = 1:3, 1.2 ml h^{-1}) was vaporised and mixed with CO_2 + H_2 (CO_2:H_2 = 11:1, 3.6×10^3 ml h^{-1}) and delivered to the reactor. A co-current flow of MeOH, NB and CO_2/H_2 was maintained at $GHSV = 2 \times 10^4$ h^{-1} with $F_{MeOH} = 1 \times 10^{-2}$ mol h^{-1} and F_{NB} = 9×10^{-2} mol h^{-1}. Passage of MeOH and/or NB in a stream of CO_2 and H_2 through the empty reactor did not result in any detectable conversion. The total mass of catalyst was divided into 2 beds for the reaction with double-bed arrangement, where the inlet reactants flow rates were kept constant. The fractional conversion of NB (X_{NB}) and DMC (X_{DMC}) was defined as

$$X_{\mathrm{NB}} = \frac{2 \times C_{\mathrm{AN,out}}}{C_{\mathrm{NB,in}}} \qquad \textbf{(3.4)}$$

$$X_{\mathrm{DMC}} = \frac{2 \times C_{\mathrm{MPC,out}}}{C_{\mathrm{DMC,in}}} \qquad \textbf{(3.5)}$$

3.2.3.3 Analytical Method and Activity/Selectivity Evaluation

The reactor effluent was analysed by capillary GC (Perkin-Elmer Auto System XL gas chromatograph equipped with a programmed split/split less injector and FID)

using a Stabilwax (fused silica) 30 m × 0.32 mm i.d., 0.25 μm film thickness capillary column (RESTEK) employing Turbo-Chrom Workstation Version 6.3.2 (for Windows) for data storage and manipulation. Quantitative analysis of reactants/products in the mixture was based on detailed calibration plots (not shown) where analytical reproducibility was better than ±8%. Repeated reactions with different samples from the same batch of catalyst delivered conversion and selectivity values that were reproducible to within ±6%. Carbon mass balance was complete to better than ±12%.

3.3 Results and Discussion

3.3.1 Catalyst Structure Characterisation

The XRD patterns for CeO_2 as prepared (**Figure 3.2(I)**) and calcined at 423 K **(II)**, 673 K **(III)** and 873 K **(IV)** show eight main peaks at 28.5°, 33.2°, 47.5°, 56.3°, 59.0°, 69.4°, 76.7° and 79.0° that correspond to the main planes of a cubic fluorite structure (**Figure 3.2(V)**).

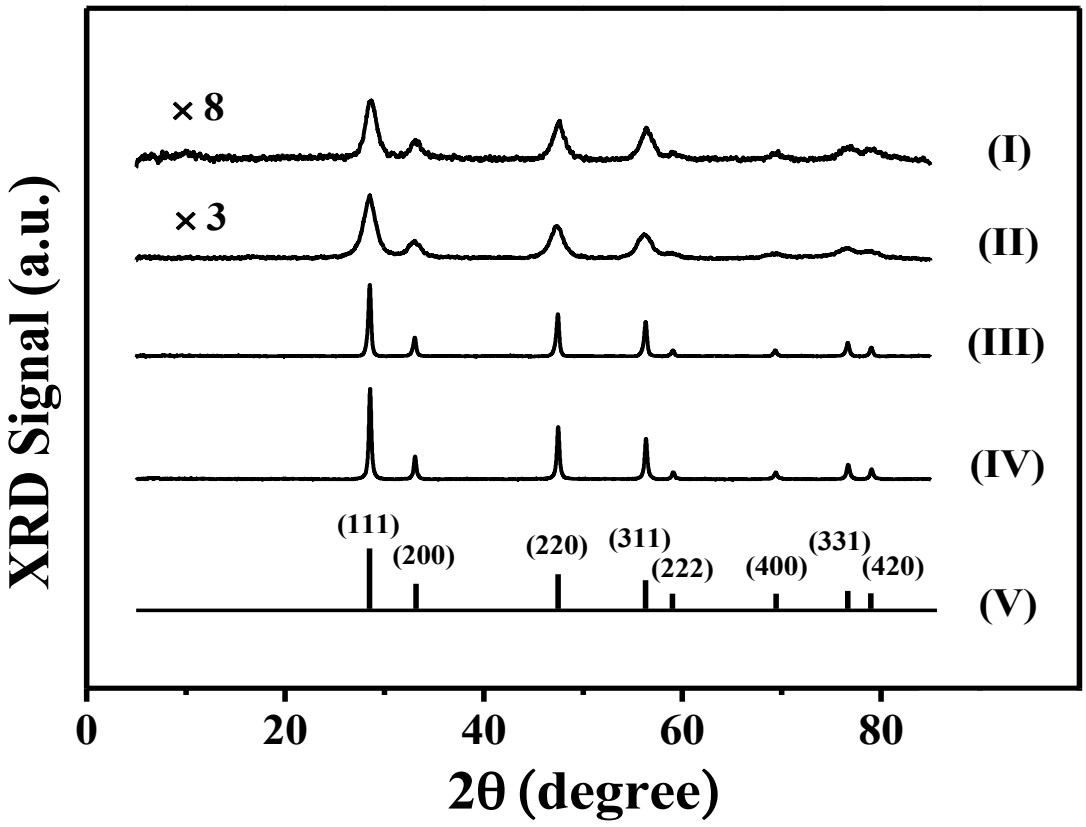

Figure 3. 2: XRD patterns for CeO_2 (I) as prepared and calcined at (II) 423 K, (III) 673 K, (IV) 873 K and (V) JCPDS-ICDD reference standard for CeO_2 (43-1002).

The similar position and peak relative intensity for all the samples indicates that CeO_2 crystal phase was not affected by calcination temperature. We observe an increase in particle size for synthesized (from 9 nm → 14 nm) and commercial (from 14 nm → 16 nm) CeO_2 samples following calcination to 873 K that agrees with reported literature [47]. Li *et al.* [48] reported that with increase in calcination temperature the crystallite size of CeO_2 showed an exponential dependence, indicating that crystallite growth is diffusion related. The smaller particle size of the synthesized CeO_2 (9 *vs.* 14 nm) was attributed to the longer aging time during preparation (60 vs. 10 h [41]) and resulted in greater SSA (119 *vs.* 52 m^2g^{-1}). An increase in SSA may be attributed to the further division of ceria into thinner slices after long time interaction with water molecules [49]. The variation of SSA with calcination temperature is presented in **Figure 3.3**, where a decline of 45 and 23% was recorded with an increase in temperature for the synthesized and commercial CeO_2, respectively.

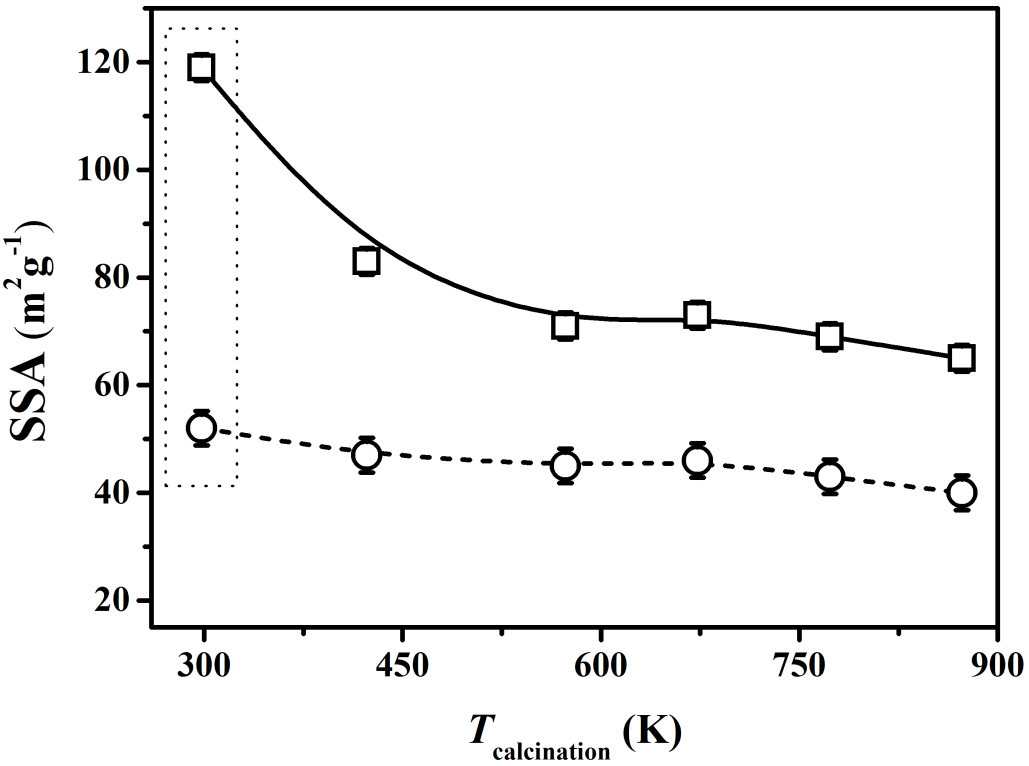

Figure 3. 3: Variation of specific surface area (SSA) with calcination temperature ($T_{calcination}$) for CeO_2-comm (○, dashed line) and CeO_2 (□, solid line). *Note*: dotted box indicates response over the fresh samples while error bars represent standard error of the mean obtained from 3 experiments.

These values falls in the range 13 – 51% quoted in literature [37] and can be ascribed to the sintering of the catalysts. Fine particles have an ability to agglomerate due to their high surface energy. This tendency becomes stronger at higher temperatures [49]. Since the sinterability of ceria favours smaller particle size [50], a lesser decrease in SSA was recorded for CeO_2-comm, which was also attributed to the negligible change in crystallite size.

3.3.2 Catalyst Surface Characterisation

The Ce 3d spectra for Pd/CeO_2-comm, and fresh and calcined CeO_2 are shown in **Figure 3.4**. The XPS profiles present three $3d_{3/2}$-$3d_{5/2}$ spin-orbit-split duplets with binding energies (BE) at **(A)** 907.0 and 888.2 eV, **(B)** 900.0 and 881.7 eV and **(C)** 916.0 and 897.4 eV that represent different 4f configurations of Ce^{4+} (*i.e.* **(A)** Ce $3d^9 4f^1$ O $2p^5$, **(B)** Ce $3d^9 4f^2$ O $2p^4$ and **(C)** Ce $3d^9 4f^0$ O $2p^6$ final states). Signals at **(D)** 901.1 and 884.0 eV, **(E)** 898.2 and 880.6 eV provide evidence for the formation of Ce^{3+} on all of the samples [51]. The Ce^{3+}/Ce^{4+} ratios (presented in **Table 3.1**) were calculated from XPS $Ce^{3+}/ (Ce^{4+} + Ce^{3+})$ ratio following the procedure established elsewhere [52], where Ce^{4+} = **(A)** + **(B)** + **(C)** and Ce^{3+} = **(D)** + **(E)**. The values obtained fall in a range between 0.1 and 0.5 quoted in the literature [53, 54] with associated experimental error below 0.02.

Table 3. 1: CO_2 desorbed (from TPD analysis) and Ce^{3+}/Ce^{4+} molar ratio (based on XPS) for commercial (CeO_2-comm) and homemade (CeO_2) ceria and Pd/CeO_2-comm.

Catalyst	CO_2 desorbed (μmol m^{-2})	Ce^{3+}/Ce^{4+}
CeO_2-comm[a]	1.2	0.23
CeO_2-comm[b]	0.8	0.14
CeO_2[a]	7.7	0.31
CeO_2[b]	4.8	0.16
Pd/CeO_2-comm	-	0.48

[a]fresh sample.
[b]sample calcined at 873 K.

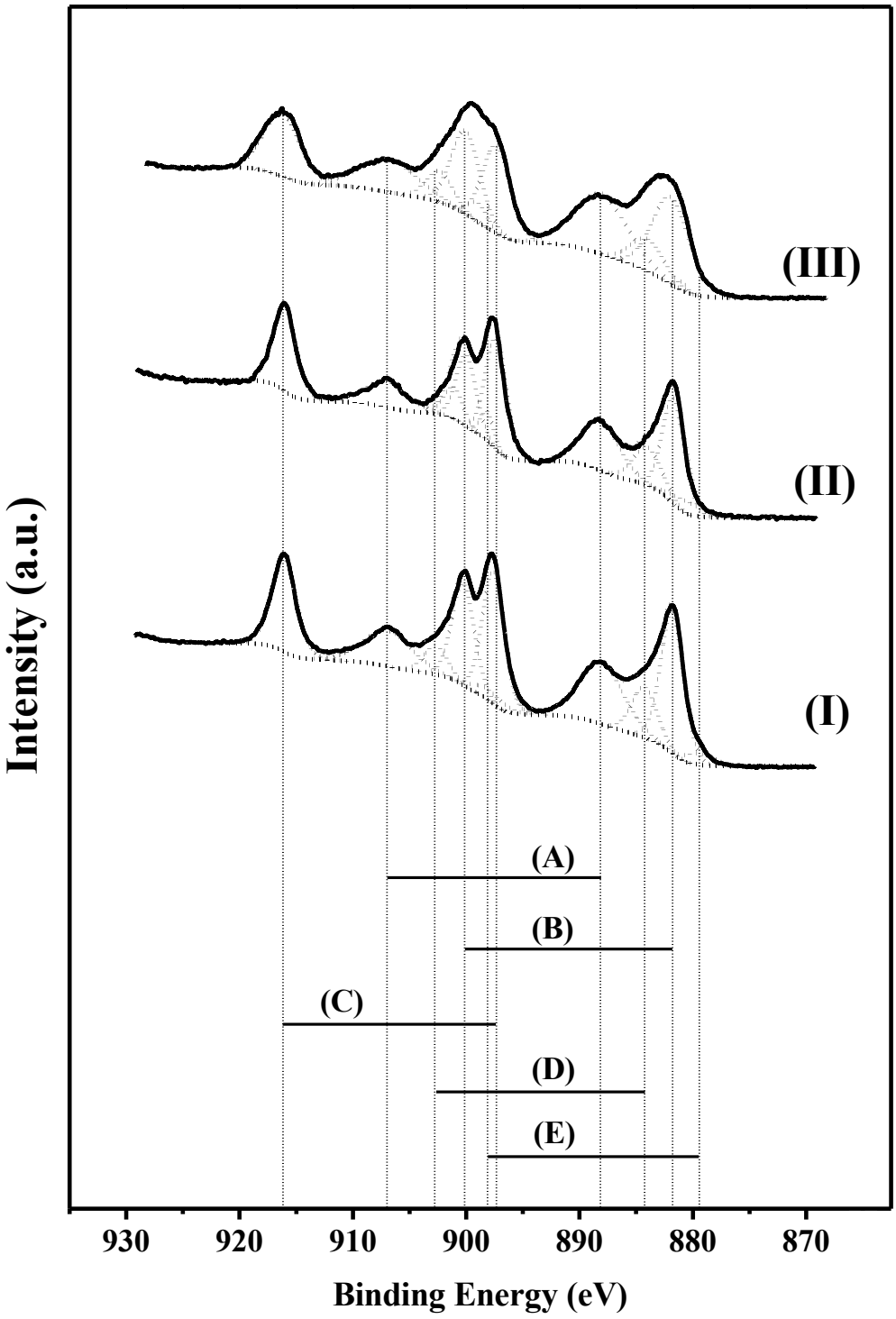

Figure 3. 4: XPS spectra for (I) Pd/CeO_2-comm and (II) fresh and (III) calcined at 873 K CeO_2 with associated 4*f* configurations for Ce^{4+} (A-C) and Ce^{3+} (D-E). *Note*: the lines represent the XPS experimental data (solid line) and peaks after deconvolution (dotted line).

It should be noted that the highest relative Ce^{3+} content in Pd/CeO_2 suggests partial support reduction as noted elsewhere [55]. Because CeO_2 is reducible support the reduction of Pd during TPR will cause the generation of oxygen vacancies (the loss of structural oxygen from the oxide sub-lattice [56]) which corresponds to the partial reduction of Ce^{4+} to Ce^{3+} cations. Greater enrichment in Ce^{3+} for the lab synthesised CeO_2 is attributed to the preparation method of the catalyst. Since the oxidation of the precipitant $Ce(OH)_3$ to $Ce(OH)_4$ in air is slow, the dehydration of $Ce(OH)_3$ starts to take place along with the oxidation step to form Ce^{3+}. Both commercial and synthesized CeO_2 showed a decrease in Ce^{3+} content after calcination (**Table 3.1**), suggesting the oxidation to Ce^{4+} species.

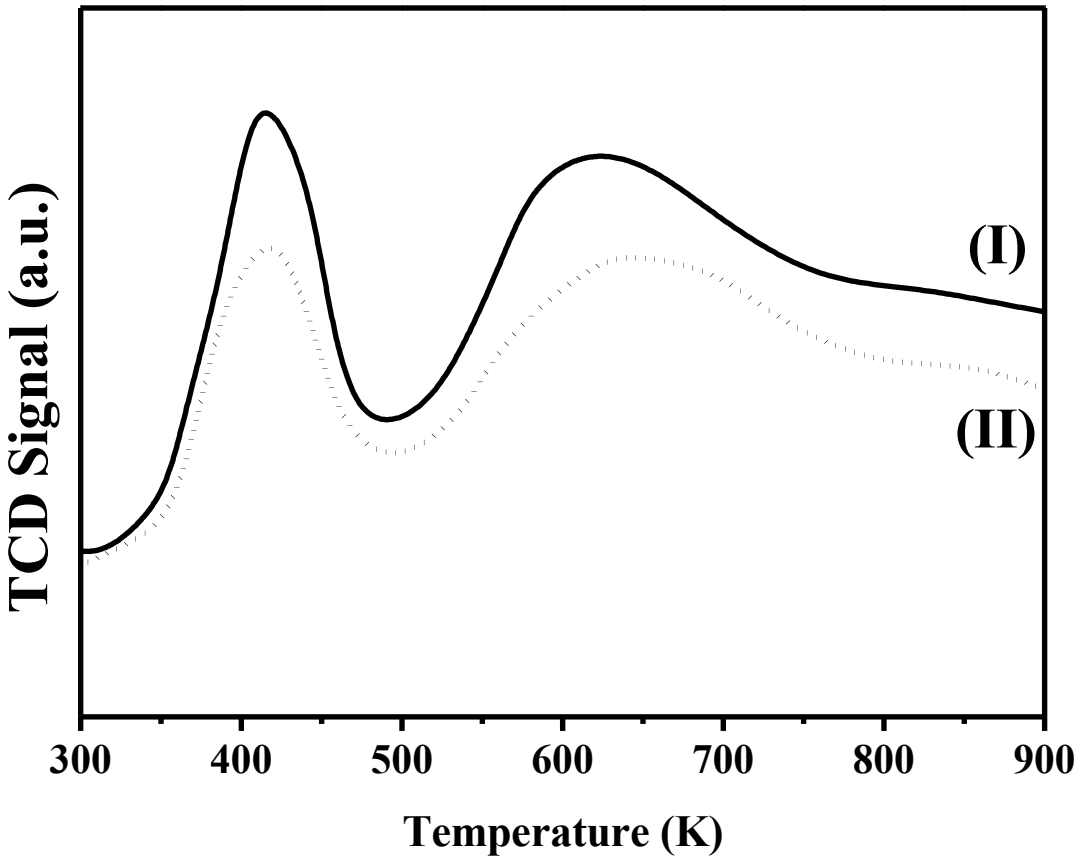

Figure 3. 5: CO_2-TPD profiles recorded for (I) fresh and (II) calcined at 873 K CeO_2-comm.

Total surface basicity was determined from CO_2-TPD (**Figure 3.5)** and CO_2 desorbed (per SSA) is given in **Table 3.1**. Both catalysts exhibited two desorption peaks

over low (≤500 K) and high (500-723 K) temperature range, characteristic of weak and moderate basic sites, respectively [57]. Surface basicity in the case of as received sample is mainly attributed to Lewis sites (Ce^{3+}), oxide (O^{2-}) ions and residual OH-groups [34] while the amount of CO_2 desorbed (1.2 μmol m^{-2}) is in a good agreement with the literature (1.9 μmol m^{-2} [58]). Lower CO_2 desorption on calcined CeO_2-comm (0.8 μmol m^{-2}, **Table 3.1**) is associated with a removal of -OH groups from the surface, resulting in oxidation of Ce^{3+} to Ce^{4+}. The amount of CO_2 desorbed from as prepared/calcined synthesised CeO_2 samples was much higher relative to CeO_2-comm. ones (**Table 3.1**), which is attributed to the greater O^{2-} and Ce^{3+} content (confirmed by XPS).

3.3.3 Optimisation of Dimethyl Carbonate Production (step I)

3.3.3.1 Effect of Calcination Temperature on Liquid phase Catalytic Dimethyl Carbonate Production

We first examine the effect of calcination temperature on the rate of DMC production and the results are presented in **Figure 3.6**. Both commercial and synthesised CeO_2 catalysts exhibited a continuous increase in specific rate (normalised with respect to SSA) with calcination temperature (from 423 to 873 K). Yoshida *et al.* [37] also showed increased rate of carbonate formation at higher calcination temperature over CeO_2, a result they ascribed to the change in SSA. We established (by XPS) that calcination is modifying these surface properties of CeO_2, *i.e.* Ce^{3+} (Lewis base) to Ce^{4+} (Lewis acid) ratio. The result obtained indicates that Ce^{4+} is an active site of the reaction. Jung *et al.* [59] proposed the mechanism for ZrO_2, where methanol dissociates on the Lewis acid (LWA) site (Zr^{4+}) to form CH_3O-Zr group with release of a H atom and CO_2 adsorbs through the C atom on the Lewis base (LWB) site (O^{2-}) and through the oxygen at Zr^{4+} cation. The proximity of the methoxide oxygen to the carbon of CO_2 enable transfer to form CH_3OCOO-Zr. Once another molecule of methanol is adsorbed in identical way, DMC is formed by transfer of a methyl group to the terminal O atom of methyl carbonate species. This mechanism revealed that the cooperation of both acid and base sites is required for CO_2 activation, *i.e.* Ce^{4+} and O^{2-} for CeO_2.

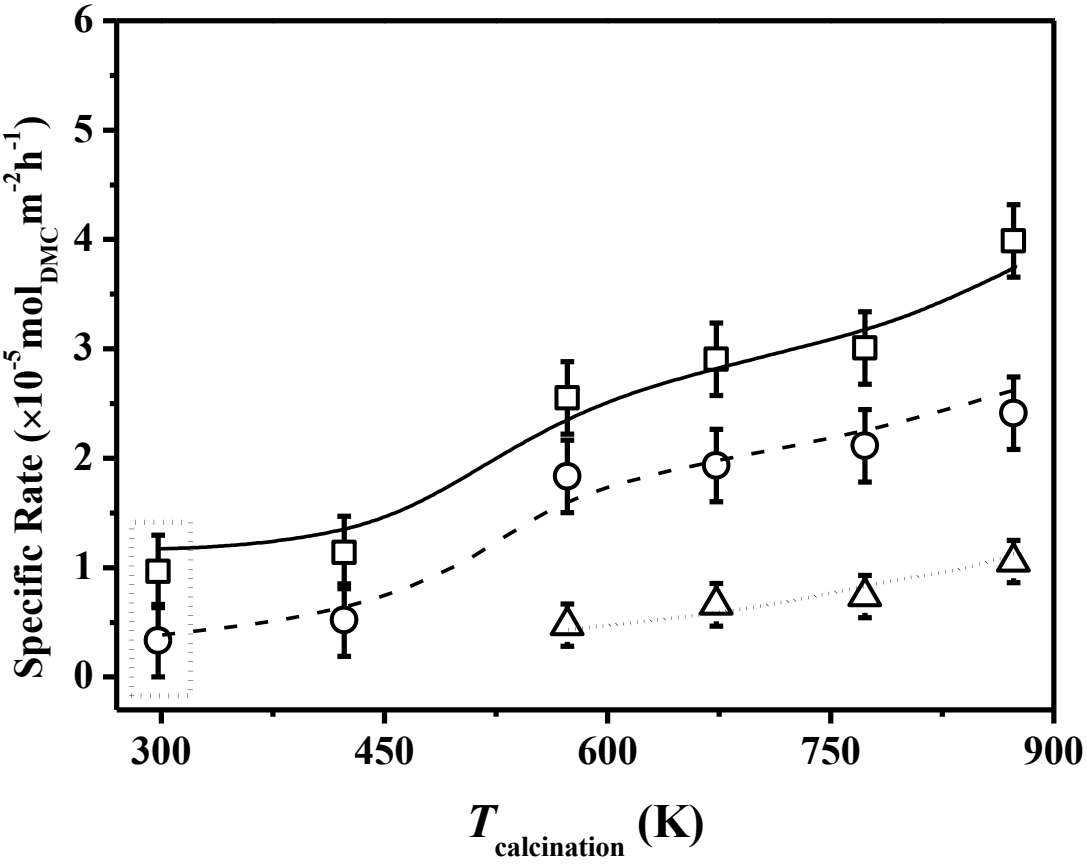

Figure 3. 6: Variation of specific (per m^2) rate of DMC production with calcination temperature ($T_{calcination}$) for reaction over CeO_2-comm (○, dashed line), CeO_2 (□, solid line) and Pd/CeO_2-comm (△, dotted line). *Note*: response over samples as prepared (or as received) is contained within the dotted box while error bars represent standard error of the mean obtained from 3 experiments.

In order to support this statement and understand the role of ceria redox properties, we tested Pd/CeO_2-comm with higher Ce^{3+}/Ce^{4+} ratio (**Table 3.1**) and lower O^{2-} content (based on O_2 chemisorption, **Table 3.2**) relative to CeO_2–comm. The rate of reaction over Pd/CeO_2-comm was a factor of two times lower. The specific rate of DMC production obtained over CeO_2 calcined at 873 K (4×10^{-5} mol_{DMC} m^{-2} h^{-1}) is similar to the maximum value quoted in literature for DEC (3.5×10^{-5} mol_{DEC} m^{-2} h^{-1}, [36]) at the same reaction conditions ($T = 423$ K; $P_{CO_2} = 5$ atm). Since Ce^{3+}/Ce^{4+} ratio is controlling the DMC production rate and both synthesized/commercial CeO_2 calcined at 873 K

delivered the equivalent values, CeO_2-comm was chosen as test catalyst for gas phase reactions.

Table 3. 2: O_2 chemisorption and reaction rates (*R*) for reaction at 723 K over CeO_2-comm and Pd/CeO_2-comm.

Catalyst	O_2 chemisorption ($\mu mol\ g^{-1}$)	*R* ($\times 10^{-5}\ mol_{DMC/AN} m^{-2} h^{-1}$)		
		Step I $CO_2 \rightarrow DMC$	Step II NB→AN	Step III DMC→MPC
CeO_2-comm	0	33	-	82
Pd/CeO_2-comm	4.1	11	1×10^{8}	78

DMC = dimethyl carbonate; NB = nitrobenzene; AN = aniline; MPC = methyl N-phenyl carbamate.

3.3.3.2 Gas Phase Catalytic Dimethyl Carbonate Production

Continuous DMC production in gas phase offers the possibility of continuous carbonate formation at atmospheric pressure in the absence of dehydrating agents [29]. A range of catalysts (*i.e.* Cu-based solid catalysts [60-62] or $Co_{1.5}PW_{12}O_{40}$ [61, 62]) have been tested in gas phase systems under 1-12 atm reaction pressures. However, the yields and DMC selectivities are below 10 and 91%, respectively, where the main by-products were dimethoxy methane and methyl formate. Full selectivity to DMC at ambient pressure in continuous gas phase operation has not been reported.

DMC was generated as the sole product at a rate of $8 \times 10^{-5}\ mol_{DMC} m^{-2} h^{-1}$, which is the highest rate of specific DMC formation from CO_2 over reported in the literature ($2.2 \times 10^{-5}\ mol_{DMC} m^{-2} h^{-1}$ [36] at 423K and 2 atm). The switch of operation mode from batch to continuous resulted in significant rate improvement (from 2.4 to $8 \times 10^{-5}\ mol_{DMC} m^{-2} h^{-1}$) that is attributed to more effective water removal from the active sites of the catalyst in gas phase causing the shift of the equilibrium.

3.3.3.3 Effect of Variation of CO_2/MeOH Ratio, Contact Time and Temperature on DMC Production Rate in Gas Phase

The documented gas phase catalytic methanol carboxylation studies have all been conducted where methanol was in excess [42] or near stoichiometric [61, 62] quantities, however an increase of CO_2 content in the feed can serve to enhance surface CO_2 which should promote the formation of DMC. The effect of varying the inlet CO_2/MeOH was examined over CeO_2-comm and the results are presented in **Figure 3.7**.

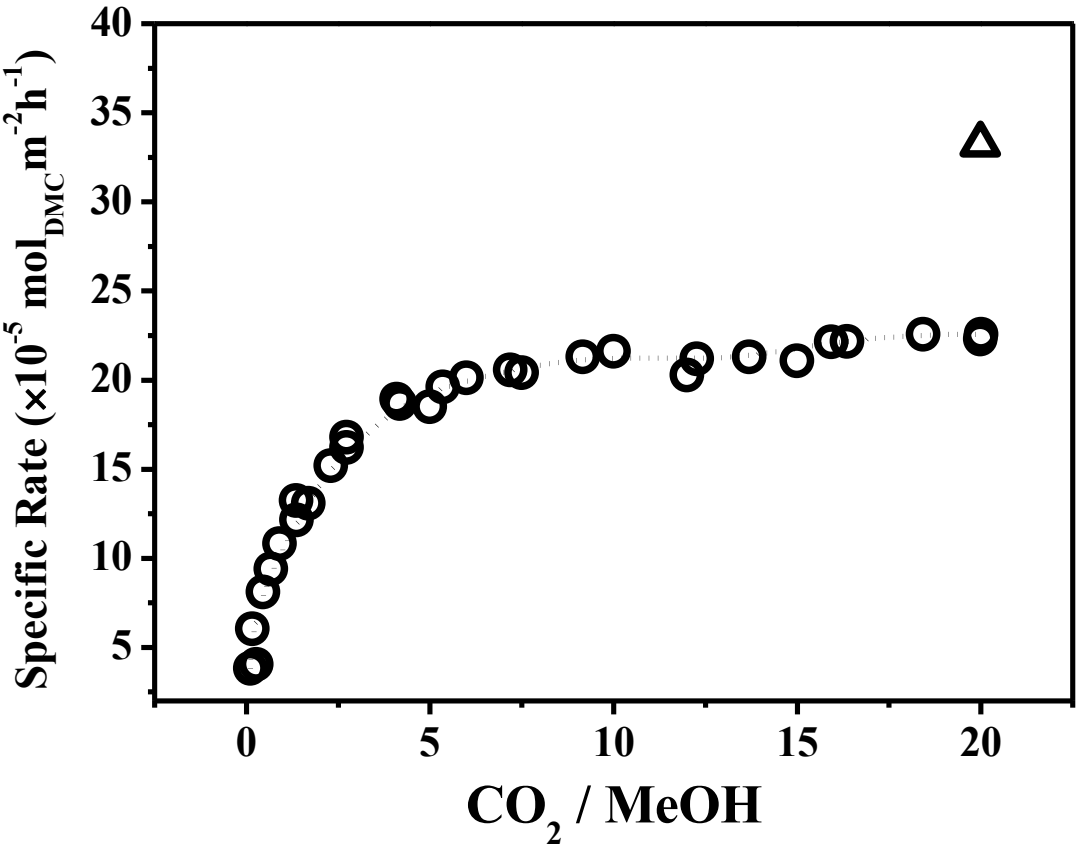

Figure 3. 7: Specific DMC formation rate (per m^2) as a function of CO_2/MeOH ratio in reaction over CeO_2-comm calcined at 873 K. *Reaction conditions*: *T* = 573 K (triangle, *T* = 723 K); *P* = 1 atm.

An initial change of CO_2/MeOH (from 0.5 to 5) resulted in a steep improvement of the initial DMC production rate from 8 to 19 × 10^{-5} $mol_{DMC}m^{-2}h^{-1}$. The volume of MeOH was reduced to further increase CO_2/MeOH in the system (from 5 to 20) while

the volume of CO_2 was kept constant. Only a slight increase in the rate up to 22×10^{-5} $mol_{DMC}m^{-2}h^{-1}$ was observed (**Figure 3.7)**, meaning that the rate becomes insensitive at higher CO_2/MeOH since maximum surface coverage with CO_2 has been achieved. The effect of the reaction temperature on the initial DMC production rate has been considered for the optimum conditions (CO_2/MeOH = 20), where the change from 573 to 723 K resulted in an increase of the rate from 22 to 33×10^{-5} $mol_{DMC}m^{-2}h^{-1}$. Under the same reaction conditions Pd/CeO_2-comm showed lower DMC production rate relative to CeO_2-comm (11 *vs.* 33×10^{-5} $mol_{DMC}m^{-2}h^{-1}$, **Table 3.2**). This was attributed to the higher Ce^{3+} content (**Table 3.1**) and O_2 chemisorption (**Table 3.2**). It should be also stressed out that the CO_2 content in the feed did not influence product composition and reaction exclusivity to DMC was maintained at each CO_2/MeOH.

3.3.4 Gas Phase Single-Pot Formation of Methyl N-Phenyl Carbamate

The highest rate of DMC formation was achieved over CeO_2-comm at 723 K, while the NB conversion to AN was only detected over Pd/CeO_2-comm (**Table 3.2**). The condensation reaction of AN with DMC was performed over both catalysts and the results obtained (82 and 78×10^{-5} $mol_{DMC}m^{-2}h^{-1}$ for CeO_2-comm and Pd/CeO_2-comm respectively, **Table 3.2**) suggest that the rate of MPC formation is insensitive to the oxidation state of ceria and to the presence of the metal. Taking into account all the requirements for the three steps involved in the formation of MPC the single-pot reaction was performed over each catalyst and the results with schematic illustration of product distribution are presented in the **Figure 3.8**. The single-pot reaction over CeO_2-comm was fully selective to DMC. Ceria does not chemisorb hydrogen [55] and did not promote the formation of AN and MPC. DMC production rate was not affected by the presence of NB or hydrogen in the feed. In order to check the possibility of the condensation reaction (step III, **Figure 3.1**) in single-pot over CeO_2-comm, NB and H_2 were substituted with AN and N_2 (**Figure 3.8(IB)**). Although, the rate of DMC formation (35×10^{-5} $mol_{DMC}m^{-2}h^{-1}$) was not affected, MPC has not been formed. The same single-pot reaction over Pd/CeO_2-comm with NB (**IIA**) or AN (**IIB**) in the feed showed lower DMC formation rate relative

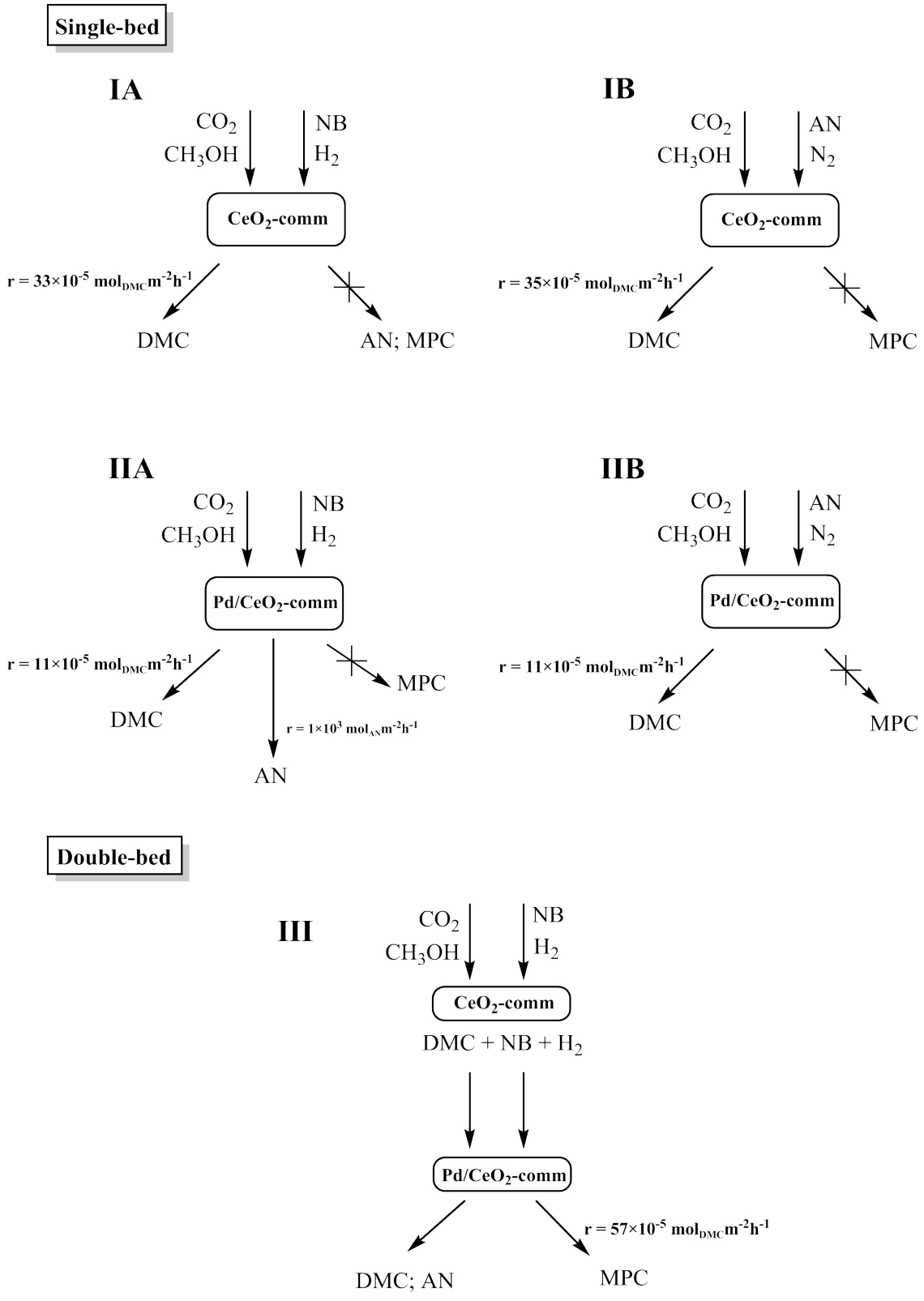

Figure 3. 8: Single ((I) CeO_2-comm and (II) Pd/CeO_2-comm) and double (III) catalyst bed reaction arrangement with associated products from inlet (A) NB + H_2 and (B) AN + N_2 reactants. *Acronyms:* nitrobenzene (NB), aniline (AN), dimethyl carbonate (DMC), methyl-N-phenyl carbamate (MPC).

to CeO_2-comm (11 *vs.* 33-35 × 10^{-5} $mol_{DMC}m^{-2}h^{-1}$), which correlates with the results obtained for the reaction of DMC formation from CO_2 and MeOH (Step I, **Figure 3.1**). The presence of palladium helped to transform NB to AN (**Figure 3.8(IIA)**), however the condensation reaction of AN with DMC has not been observed and MPC was not formed. Considering these results obtained for both CeO_2-comm and Pd/CeO_2-comm, we suggest that activation of CO_2 involves the initial formation of an intermediate with sequential transformation to DMC. This intermediate is required for the condensation reaction with AN to form MPC. However, as DMC is formed during the reaction, it leaves the surface of the catalyst and condensation with AN does not occur.

Operation of a second catalyst bed with Pd/CeO_2-comm in series should facilitate the conversion of DMC exiting the first bed by reaction with AN generated *via* NB hydrogenation in the second bed. This will lead to the formation of MPC. A simplified schematic diagram of the double-bed arrangement and corresponding product distribution is presented in **Figure 3.8(III)**. MPC has been produced (57 × 10^{-5} $mol_{DMC}m^{-2}h^{-1}$) along with unreacted DMC and AN. This is the first time that the production of MPC from CO_2 has been reported over both continuous and batch modes of operation.

3.4 Conclusions

We have achieved MPC production in a continuous single-pot process operated at atmospheric pressure using CO_2, methanol and NB. We studied the effect of calcination of CeO_2 on the specific carboxylation rate and the highest rate was achieved at 873 K for liquid operation mode. We have established that catalytic performance for DMC production is dependent predominantly on the redox properties of CeO_2 (surface Ce^{3+}/Ce^{4+} ratio) rather than SSA. CO_2-TPD revealed the presence of weak-moderate surface basicity, which was mainly attributed to Ce^{3+} sites. The effect of Pd incorporation resulted in an increase of Ce^{3+} surface content (by partial oxide reduction during TPR), which lowered catalytic activity towards DMC formation. This result indicates on the requirement of surface O^{2-} and Ce^{4+} species for the activation of CO_2, which is also supported by an increase in the specific rate with calcination temperature.

In the gas phase continuous mode, 100% selectivity to the target DMC was achieved over CeO_2-comm (calcined at 873K) with the highest rate (8×10^{-5} mol_{DMC} m^{-2} h^{-1} in respect to SSA) quoted in the literature. The effect of varying the inlet CO_2/MeOH (0.5 – 20) and the reaction temperature (573 – 723 K) over CeO_2-comm helped to further improve the initial DMC production rate from 8 to 33×10^{-5} $mol_{DMC}m^{-2}h^{-1}$. MPC was achieved (at rate 57×10^{-5} $mol_{DMC}m^{-2}h^{-1}$) over a double-bed (CeO_2-comm on top and Pd/CeO_2-comm in the bottom) arrangement.

3.5 References

[3.1] G.A. Olah, G.K.S. Prakash and A. Goeppert, *Anthropogenic Chemical Carbon Cycle for a Sustainable Future.* J. Am. Chem. Soc., 2011. **133**: p. 12881-12898.

[3.2] C. Genovese, C. Ampelli, S. Perathoner and G. Centi, *Electrocatalytic Conversion of CO_2 to Liquid Fuels Using Nanocarbon-Based Electrodes.* J. Energy Chem., 2013. **22**: p. 202-213.

[3.3] M. Aresta, A. Dibenedetto and A. Angelini, *The Changing Paradigm in CO_2 Utilization.* J. CO_2 Util., 2013. **3–4**: p. 65-73.

[3.4] G. Centi and S. Perathoner, *Opportunities and Prospects in the Chemical Recycling of Carbon Dioxide to Fuels.* Catal. Today, 2009. **148**: p. 191-205.

[3.5] J.F. Hull, Y. Himeda, W.-H. Wang, B. Hashiguchi, R. Periana, D.J. Szalda, J.T. Muckerman and E. Fujita, *Reversible Hydrogen Storage Using CO_2 and a Proton-Switchable Iridium Catalyst in Aqueous Media under Mild Temperatures and Pressures.* Nat. Chem., 2012. **4**: p. 383-388.

[3.6] A. Bansode and A. Urakawa, *Towards Full One-Pass Conversion of Carbon Dioxide to Methanol and Methanol-Derived Products.* J. Catal., 2014. **309**: p. 66-70.

[3.7] C.J. Whiteoak, N. Kielland, V. Laserna, F. Castro-Gómez, E. Martin, E.C. Escudero-Adán, C. Bo and A.W. Kleij, *Highly Active Aluminium Catalysts for the Formation of Organic Carbonates from CO_2 and Oxiranes.* Chem. Eur. J., 2014. **20**: p. 2264-2275.

[3.8] J. Sun, B. Lu, X. Wang, X. Li, J. Zhao and Q. Cai, *A Functionalized Basic Ionic Liquid for Synthesis of Dimethyl Carbonate from Methanol and CO_2.* Fuel

Process. Technol., 2013. **115**: p. 233-237.

[3.9] H. An, L. Zhang, B. Yuan, X. Zhao and Y. Wang, *Influence of Solvent on Reaction Path to Synthesis of Methyl N-Phenyl Carbamate from Aniline, CO_2 and Methanol.* Chin. J. Chem. Eng., 2014. **22**: p. 607-610.

[3.10] C.N. Tang, H.B. Nulwala, K. Damodaran, P. Kaur and D.R. Luebke, *Tunable Poly(Hydroxyl Urethane) from CO_2-Based Intermediates Using Thiol-Ene Chemistry.* J. Polym. Sci., Part A: Polym. Chem., 2011. **49**: p. 2024-2032.

[3.11] T. Mita, Y. Higuchi and Y. Sato, *Highly Regioselective Palladium-Catalyzed Carboxylation of Allylic Alcohols with CO_2.* Chem. Eur. J., 2015. **21**: p. 16391-16394.

[3.12] W.N.R.W. Isahak, Z.A.C. Ramli, M.W.M. Hisham and M.A. Yarmo, *The Formation of a Series of Carbonates from Carbon Dioxide: Capturing and Utilisation.* Renew. Sust. Energ. Rev., 2015. **47**: p. 93-106.

[3.13] N. Yang and R. Wang, *Sustainable Technologies for the Reclamation of Greenhouse Gas CO_2.* J. Clean Prod., 2015. **103**: p. 784-792.

[3.14] S.-H. Pyo, P. Persson, M.A. Mollaahmad, K. Sörensen, S. Lundmark and R. Hatti-Kaul, *Cyclic Carbonates as Monomers for Phosgene- and Isocyanate-Free Polyurethanes and Polycarbonates*, Pure Appl. Chem., 2011. **84** p. 637-661.

[3.15] W. Yang, Q. Dong, S. Liu, H. Xie, L. Liu and J. Li, *Recycling and Disposal Methods for Polyurethane Foam Wastes*, Procedia Environ. Sci., 2012. **16**: p. 167-175.

[3.16] J. Gao, H. Li, Y. Zhang and Y. Zhang, *A Non-Phosgene Route for Synthesis of Methyl N-Phenyl Carbamate Derived from CO_2 Under Mild Conditions.* Green Chem., 2007. **9**: p. 572-576.

[3.17] B. Wan, S. Liao and D. Yu, *Polymer-Supported Palladium–Manganese Bimetallic Catalyst for the Oxidative Carbonylation of Amines to Carbamate Esters*. Appl. Catal., A, 1999. **183**: p. 81-84.

[3.18] B. Chen and S.S.C. Chuang, *$CuCl_2$ and $PdCl_2$ Catalysts for Oxidative Carbonylation of Aniline with Methanol.* J. Mol. Catal. A: Chem., 2003. **195**: p. 37-45.

[3.19] F. Ragaini and S. Cenini, *Mechanistic Study of the $Ru_3(CO)_{12}$/Chloride Catalyzed Carbonylation Reactions of Nitroarenes to Carbamates and Ureas; the Role of the Alkylammonium Cation.* J. Mol. Catal. A: Chem., 2000. **161**: p. 31-38.

[3.20] F. Ragaini, M. Gasperini and S. Cenini, *Phosphorus Acids as Highly Efficient Promoters for the Palladium-Phenanthroline Catalyzed Carbonylation of Nitrobenzene to Methyl Phenylcarbamate.* Adv. Synth. Catal., 2004. **346**: p. 63–71.

[3.21] X. Zhao, Y. Wang, S. Wang, H. Yang and J. Zhang, *Synthesis of MDI from Dimethyl Carbonate over Solid Catalysts.* Ind. Eng. Chem. Res., 2002. **41**: p. 5139–5144.

[3.22] B. Chen and S.S.C. Chuang, *In Situ Infrared Study of Oxidative Carbonylation of Aniline with Methanol on Cu-Based Catalysts*. Green Chem., 2003. **5**: p. 484-489.

[3.23] M. Abla, J.C. Choi and T. Sakakura, *Halogen-Free Process for the Conversion of Carbon Dioxide to Urethanes by Homogeneous Catalysis.* Chem. Commun., 2001. **1**: p. 2238-2239.

[3.24] M. Abla, J.C. Choi and T. Sakakura, *Nickel-Catalyzed Dehydrative Transformation of CO_2 to Urethanes.* Green Chem., 2004. **6**: p. 524-525.

[3.25] A. Ion, C.V. Doorslaer, V. Parvulescu, P. Jacobs and D.D. Vos, *Green Synthesis of Carbamates from CO_2, Amines and Alcohols*. Green Chem., 2008. **10**; p. 111-116.

[3.26] P. Sangeetha, K. Shanthi, K.S.R. Rao, B. Viswanathan and P. Selvam, *Hydrogenation of Nitrobenzene over Palladium-Supported Catalysts—Effect of Support.* Appl. Catal., A, 2009. **353**: p. 160-165.

[3.27] S. Diao, W. Qian, G. Luo, F. Wei and Y. Wang, *Gaseous Catalytic Hydrogenation of Nitrobenzene to Aniline in a Two-Stage Fluidized Bed Reactor.* Appl. Catal., A, 2005. **286**: p. 30-35.

[3.28] N. Katada, H. Fujinaga, Y. Nakamura, K. Okumura, K. Nishigaki and M. Niwa, *Catalytic Activity of Mesoporous Silica for Synthesis of Methyl N-Phenyl*

Carbamate from Dimethyl Carbonate and Aniline. Catal. Lett., 2002. **80**: 47-51.

[3.29] M. Honda, M. Tamura, Y. Nakagawa and K. Tomishige, *Catalytic CO_2 Conversion to Organic Carbonates with Alcohols in Combination with Dehydration System.* Catal. Sci. Technol., 2014. **4**: p. 2830-2845.

[3.30] Q. Cai, C. Jin, B. Lu, H. Tangbo and Y. Shan, *Synthesis of Dimethyl Carbonate from Methanol and Carbon Dioxide Using Potassium Methoxide as Catalyst under Mild Conditions.* Catal. Lett., 2005. **103**: p. 225-228.

[3.31] J. Kizlink and I. Pastucha, *Preparation of Dimethyl Carbonate from Methanol and Carbon Dioxide in the Presence of Sn(IV) and Ti(IV) Alkoxides and Metal Acetates.* Collect. Czech. Chem. Commun., 1995. **60**: p. 687-692.

[3.32] H.J. Hofmann, A. Brandner and P. Claus, *Direct Synthesis of Dimethyl Carbonate by Carboxylation of Methanol on Ceria-Based Mixed Oxides.* Chem. Eng. Technol., 2012. **35**: p. 2140-2146.

[3.33] H.J. Lee, S. Park, I.K. Song and J.C. Jung, *Direct Synthesis of Dimethyl Carbonate from Methanol and Carbon Dioxide over $Ga_2O_3/Ce_{0.6}Zr_{0.4}O_2$ Catalysts: Effect of Acidity and Basicity of the Catalysts.* Catal. Lett., 2011. **141**: p. 531-537.

[3.34] E. Leino, N. Kumar, P. Mäki-Arvela, A. Aho, K. Kordás, A.-R. Leino, A. Shchukarev, D.Y. Murzin and J.-P. Mikkola, *Influence of the Synthesis Parameters on the Physico-Chemical and Catalytic Properties of Cerium Oxide for Application in the Synthesis Of Diethyl Carbonate.* Mater. Chem. Phys., 2013. **143**: p. 65-75.

[3.35] Y. Cao, H. Cheng, L. Ma, F. Liu and Z. Liu, *Research Progress in the Direct Synthesis of Dimethyl Carbonate from CO_2 and Methanol.* Catal. Surv. Asia, 2012. **16**: p. 138-147.

[3.36] M. Honda, S. Kuno, N. Begum, K.-i. Fujimoto, K. Suzuki, Y. Nakagawa and K. Tomishige, *Catalytic Synthesis of Dialkyl Carbonate from Low Pressure CO_2 and Alcohols Combined with Acetonitrile Hydration Catalyzed by CeO_2.* Appl. Catal., A, 2010. **384**: p. 165-170.

[3.37] Y. Yoshida, Y. Arai, S. Kado, K. Kunimori and K. Tomishige, *Direct Synthesis*

of Organic Carbonates from the Reaction of CO_2 with Methanol and Ethanol over CeO_2 Catalysts. Catal. Today, 2006. **115**: p. 95-101.

[3.38] K. Tomishige, H. Yasuda, Y. Yoshida, M. Nurunnabi, B. Li and K. Kunimori, *Catalytic Performance and Properties of Ceria Based Catalysts for Cyclic Carbonate Synthesis from Glycol and Carbon Dioxide.* Green Chem., 2004. **6**: p. 206-214.

[3.39] M. Aresta, A. Dibenedetto, C. Pastore, A. Angelini, B. Aresta and I. Pápai, *Influence of Al_2O_3 on the Performance of CeO_2 Used as Catalyst in the Direct Carboxylation of Methanol to Dimethylcarbonate and the Elucidation of the Reaction Mechanism.* J. Catal., 2010. **269**: p. 44-52.

[3.40] M. Aresta, A. Dibenedetto, C. Pastore, C. Cuocci, B. Aresta, S. Cometa and E. De Giglio, *Cerium(IV)Oxide Modification by Inclusion of a Hetero-Atom: A Strategy for Producing Efficient and Robust Nano-Catalysts for Methanol Carboxylation.* Catal. Today, 2008. **137**: p. 125-131.

[3.41] K. Hanawa, N. Mochizuki and N. Ueda, *Cerium Oxide Ultrafine Particles and Method for Preparing the Same*. US Patent 5938837 A, 1999.

[3.42] X. Wang, N. Perret and M.A. Keane, *Gas Phase Hydrogenation of Nitrocyclohexane over Supported Gold Catalysts.* Appl. Catal., A, 2013. **467**: p. 575-584.

[3.43] W.-J. Shen and Y. Matsumura, *Interaction Between Palladium and The Support in Pd/CeO_2 Prepared by Deposition–Precipitation Method and The Catalytic Activity for Methanol Decomposition*. J. Mol. Catal. A: Chem., 2000. **153**:p. 165-168.

[3.44] F. Cárdenas-Lizana, S. Gómez-Quero, C. Amorim and M.A. Keane, *Gas Phase Hydrogenation of p-Chloronitrobenzene over $Pd–Ni/Al_2O_3$.* Appl. Catal., A, 2014. **473**: p. 41-50.

[3.45] C.T. Campbell and C.H.F. Peden, *Oxygen Vacancies and Catalysis on Ceria Surfaces.* Science, 2005. **309**: p. 713-714.

[3.46] S. Gomez-Quero, F. Cárdenas-Lizana and M.A. Keane, *Effect of Metal Dispersion on the Liquid-Phase Hydrodechlorination of 2,4-Dichlorophenol*

over Pd/Al_2O_3. Ind. Eng. Chem. Res., 2008. **47**: p. 6841–6853.

[3.47] J.-C. Chen, W.-C. Chen, Y.-C. Tien and C.-J. Shih, *Effect of Calcination Temperature on the Crystallite Growth of Cerium Oxide Nano-Powders Prepared by the Co-Precipitation Process.* J. Alloys Compd., 2010. **496**: p. 364-369.

[3.48] J.-G. Li, T. Ikegami, J.-H. Lee, and T. Mori, *Characterization and Sintering of Nanocrystalline CeO_2 Powders Synthesized by a Mimic Alkoxide Method*. Acta Mater., 2001. **49**: p. 419-426.

[3.49] S.-H. Feng and J.-S. Chen, *Frontiers of Solid State Chemistry: Proceedings of the International Symposium on Solid State Chemistry in China*, Changchun, China, 2002. p. 191-195.

[3.50] Y. Zhou and M.N. Rahaman, *Effect of Redox Reaction on the Sintering Behavior of Cerium Oxide*, Acta Mater., 1997. **45**: p. 3635-3639.

[3.51] C.T. Nottbohm and C. Hess, *Investigation of Ceria by Combined Raman, Uv–Vis and X-Ray Photoelectron Spectroscopy.* Catal. Commun., 2012. **22**: p. 39-42.

[3.52] J.A. Hernández, S.A. Gómez, T.A. Zepeda, J.C. Fierro-González and G.A. Fuentes, *Insight into the Deactivation of Au/CeO_2 Catalysts Studied by In Situ Spectroscopy During the CO-PROX Reaction*. ACS Catal., 2015. 5: p. 4003-4012.

[3.53] G.R. Rao and H.R. Sahu, *XRD and UV-Vis Diffuse Reflectance Analysis of CeO_2-ZrO_2 Solid Solutions Synthesized by Combustion Method*. J. Chem. Sci., 2001. **113**: p. 651-658.

[3.54] H. Wang, H. Zhu, Z. Qin, F. Liang, G. Wang and J. Wang,. *Deactivation of a Au/CeO_2–Co_3O_4 Catalyst During CO Preferential Oxidation in H_2-rich Stream*. J. Catal., 2009. **264**: p. 154-162.

[3.55] D.R. Mullins, *The Surface Chemistry of Cerium Oxide.* Surf. Sci. Rep., 2015. **70**: p. 42-85.

[3.56] M. Ousmane, L.F. Liotta, G.D. Carlo, G. Pantaleo, A.M. Venezia, G. Deganello, L. Retailleau, A. Boreave and A. Giroir-Fendler, *Supported Au Catalysts for*

Low-Temperature Abatement of Propene and Toluene, as Model VOCs: Support Effect. Appl. Catal., B, 2011. **101**: p. 629-637.

[3.57] M.V. Ganduglia-Pirovano, A. Hofmann and J. Sauer, *Oxygen Vacancies in Transition Metal and Rare Earth Oxides: Current State of Understanding and Remaining Challenges.* Surf. Sci. Rep., 2007. **62**: p. 219-270.

[3.58] I. Prymak, V.N. Kalevaru, S. Wohlrab and A. Martin, *Continuous Synthesis of Diethyl Carbonate from Ethanol and CO_2 over Ce-Zr-O Catalysts.* Catal. Sci. Technol., 2015. **5**: p. 2322-2331.

[3.59] K.T. Jung and A.T. Bell, *An in Situ Infrared Study of Dimethyl Carbonate Synthesis from Carbon Dioxide and Methanol over Zirconia.* J. Catal., 2001. **204**: p. 339-347.

[3.60] X.J. Wang, M. Xiao, S.J. Wang, Y.X. Lu and Y.Z. Meng, *Direct Synthesis of Dimethyl Carbonate from Carbon Dioxide and Methanol Using Supported Copper (Ni, V, O) Catalyst with Photo-Assistance.* J. Mol. Catal. A: Chem., 2007. **278**: p. 92-96.

[3.61] A. Aouissi and S.S. Al-Deyab, *Comparative Study between Gas Phase and Liquid Phase for the Production of DMC from Methanol and CO_2.* J. Nat. Gas Chem., 2012. **21**: p. 189-193.

[3.62] A. Aouissi, Z.A. Al-Othman and A. Al-Amro, *Gas-Phase Synthesis of Dimethyl Carbonate from Methanol and Carbon Dioxide over $Co_{1.5}PW_{12}O_{40}$ Keggin-Type Heteropolyanion.* Int. J. Mol. Sci., 2010. **11**: p. 1343-1344.

Chapter 4

Catalytic Dehydration of Alcohols to Industrially Relevant Products over Ceria

In this chapter, the effect of ceria surface properties (Ce^{3+}/Ce^{4+}) on product distribution in 1-butanol/1,3-butanediol dehydration is studied, using Al_2O_3 as a benchmark. The reaction pathways and mechanisms involved are considered and discussed.

4.1 Introduction

Unsaturated (allylic and homoallylic) alcohols are important intermediates in the manufacture of aroma chemicals, pharmaceuticals, agricultural chemicals, and polymers [1]. Traditional synthesis of these compounds has been based on the use of fossil fuel derivatives [2, 3]. With an annual global production of allyl alcohol alone exceeding 14 $\times 10^5$ tonnes [4] there is an imperative need for the development of alternative ways to synthesise unsaturated alcohols. 3-Buten-2-ol (3B2OL) is an unsaturated alcohol extensively used for the production of industry-relevant chemicals (*i.e.* methyl vinyl ketone [5]). 3B2OL is industrially produced by reacting methylmagnesium iodide with 2-propenal (**Figure 4.1(I)**), also known as acrolein [6]. There are several safety and sustainability issues associated with this pathway as acrolein is highly flammable, very toxic, corrosive and dangerous for the environment [7] and is conventionally prepared by oxidation of propene [8], which is produced from fossil resources (*e.g.* petroleum, natural gas and coal [9, 10]). There are currently three alternative routes being studied for the production of 3B2OL (**Figure 4.1**): hydration of butadiene (**II**) [11], dehydration of 2,3-butanediol (**III**) [12, 13] and 1,3-butandiol (**IV**) [14-16]. The former pathway (**II**) involves using toxic and flammable butadiene [17, 18] as a reactant. Dehydration of diols (**III** and **IV**) is a most attractive option since diols are cheap, *non*-hazardous and can be produced from sustainably sourced feedstock (*i.e.* sugarcane molasses) [19, 20].

However, this process has its own challenges which are associated with the side-product formation [12, 21].

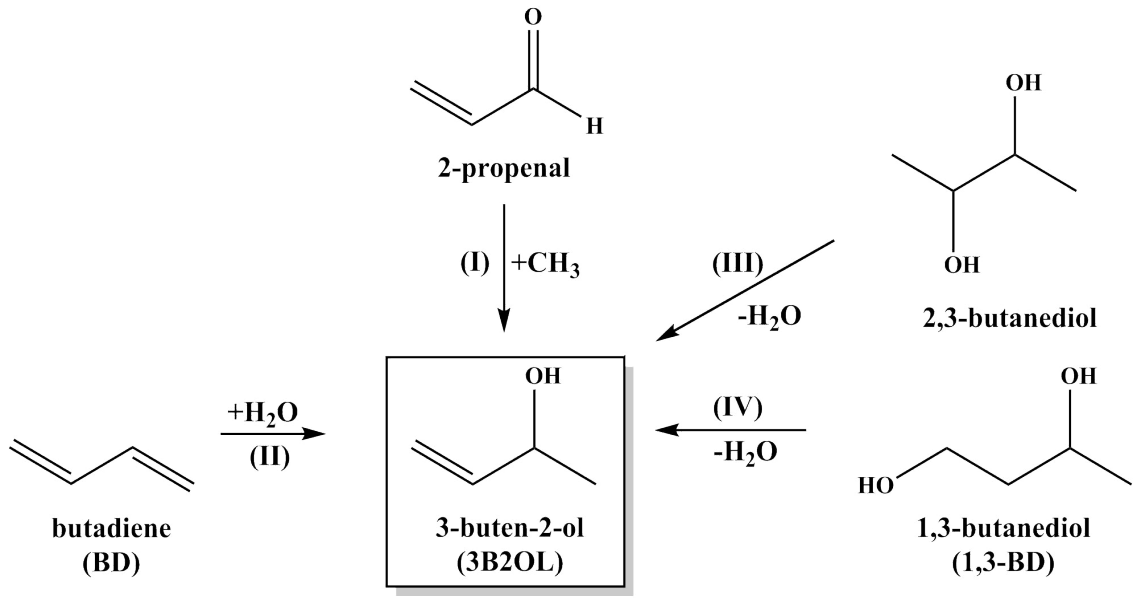

Figure 4. 1: Reaction pathways involved in 3-buten-2-ol production.

Dehydration of 1,3-BD is slightly more viable compared to 2,3-butanediol which is ascribed to the higher reported selectivity to 3B2OL (65 *vs.* 50%) [12, 21]. Reaction pathways involved in the dehydration of 1,3-BD are presented on **Figure 4.2**, where it can be seen that the dehydration of 1,3-BD can proceed *via* primary and/or secondary hydroxyl group. Since the target 3B2OL is produced by elimination of the primary hydroxyl group, the dehydration of terminal mono-alcohol (*i.e.* 1-butanol) was chosen to investigate the influencing factors on product distribution and to optimise the formation of target alkene (*i.e.* 1-butene). It has been established [22, 23] that the cooperation of both acid and base properties of the catalyst are determining in the dehydration performance. An initial activation of an alcohol on the surface of the catalyst proceeds through the adsorption of OH^- on the Lewis acid (LWA) site [12]. It has been confirmed [24, 25] that the rate of alcohol conversion increases with increasing surface (Lewis) acidity of the catalyst. Among all of the catalysts tested in 1-butanol dehydration reaction, the alumina based ones showed the highest activity (up to 100%),

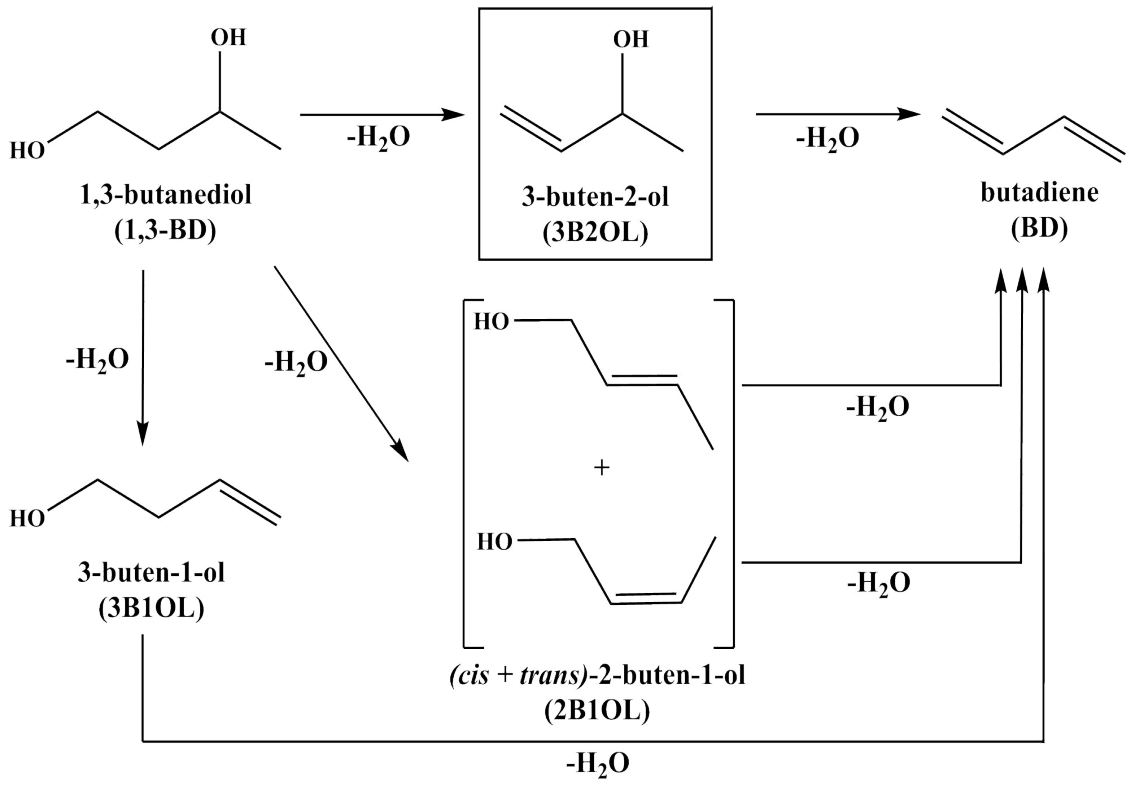

Figure 4. 2: Reaction pathways associated with 1,3-butanediol dehydration.

which was attributed to the high Lewis acidity [26, 27]. It was also demonstrated in previous chapter that the calcination treatment of cerium oxide alters the surface acid-base properties by increasing the amount of LWA sites caused by Ce^{3+} to Ce^{4+} transformation.

Taking this into account, in this study we establish the effect of modifying surface properties of ceria (Ce^{4+}/Ce^{3+}) on the catalytic activity and product distribution in 1-butanol/1,3-butanediol dehydration under continuous mode of operation, taking Al_2O_3 as a benchmark. We consider the mechanisms involved and study the effect of metal incorporation on product distribution.

4.2 Experimental

4.2.1 Catalyst Preparation

A commercial CeO_2 support was purchased from Sigma Aldrich and used as received. A 4.2% w/w Pd/CeO_2 catalyst was prepared by deposition-precipitation on

CeO_2. An aqueous solution of sodium carbonate (>99%, anhydrous, Sigma Aldrich), used as basification agent, was added (2 M, 50 cm^3, 20 cm^3 h^{-1}) to an aqueous solution of $Pd(NO_3)_2$ (2×10^{-5} M; 300 cm^3, Sigma Aldrich) containing the CeO_2 support (10 g). The suspension was stirred and pH progressively increased to reach *ca.* 10 with precipitation of $Pd(OH)_2$ [28]. A 1.1% w/w Au/CeO_2 and 0.6% w/w Ag/CeO_2 were prepared by deposition-precipitation on CeO_2 using urea as basification agent in a similar manner. An aqueous mixture of urea (*ca.* 10-fold urea excess, Riedel-de Haën, 99%) and 400 cm^3 (5×10^{-4} M) metal precursor ($HAuCl_4$ or $AgNO_3$, Sigma Aldrich) was added to the support (10 g). The suspension was stirred and heated to 353 K (2 K min^{-1}) and the pH progressively increased (from pH = 3 ~ 4) to reach *ca.* 8 after 3h as a result of thermally induced urea decomposition. The resultant solid was separated by centrifugation, washed with deionised water until the pH reached *ca.* 7 and dried in He (45 cm^3 min^{-1}) at 373 K (2 K min^{-1}) for 5 h. Prior to use, the catalysts were sieved to 75 μm average particle diameter ATM fine test sieves and activated (in H_2)/calcined (in O_2) at 2 K min^{-1} to 573–873 K. The activated samples were passivated in 1% v/v O_2/He at room temperature for *ex situ* characterisation.

4.2.2 Catalyst Characterisation

The metal content was measured by atomic absorption spectroscopy (Shimadzu AA-6650 spectrometer with an air-acetylene flame) from the diluted extract in aqua regia (25% v/v HNO_3/HCl). Temperature programmed reduction (TPR) was recorded using the commercial CHEM-BET 3000 (Quantachrome Instruments) unit equipped with a thermal conductivity detector (TCD) for continuous monitoring of gas composition and the TPR Win™ software for data acquisition/manipulation. Samples (0.05-0.1 g) were loaded into a U-shaped Quartz cell (3.76 mm i.d.), and heated in 17 cm^3 min^{-1} (Brooks mass flow controller) 5% v/v H_2/N_2 at 2 K min^{-1} to 573 K, following the reduction procedure established previously [29]. The samples were maintained at the final isothermal hold in a flow of H_2/N_2 until the signal returned to baseline, swept with a 65 cm^3 min^{-1} flow of N_2 for 1.5 h and cooled to room temperature.

4.2.3 Chemicals

1-butanol (99.8% w/w), 1,3-butanediol (≥99% w/w), 3-buten-2-ol (97% w/w), dibutyl ether (99.3% w/w), 2-buten-1-ol (96% w/w), 3-buten-1-ol (96% w/w), 3-butene-2-one (≥95% w/w), butanone (≥99% w/w) and 2-butanol (99.5% w/w) were supplied by Sigma Aldrich and used as received. All the gases (H_2, N_2, O_2 and He) were of ultra high purity (>99.99%, BOC).

4.2.4 Catalytic System

Gas phase dehydration of 1-butanol/1,3-butanediol (T = 473 – 623 K; P = 1 atm) was carried out in a fixed bed vertical continuous plug-flow glass reactor (i.d. = 12 mm). Reactant was delivered to the reactor *via* a glass/teflon air-tight syringe and a teflon line at a fixed calibrated flow rate (1.2 $cm^3\ h^{-1}$) using a microprocessor controlled infusion pump (Model 100, KD Scientific). A layer of borosilicate glass balls (2mm diameter; 3 cm height) served as preheating zone, ensure that the reactant was vaporised and reached the reaction temperature before contacting the catalyst bed. Reaction temperature was continuously monitored by a thermocouple inserted in a thermowell within the catalyst bed. A co-current flow of 1-butanol/1,3-butanediol and N_2 was maintained at $GHSV = 2 \times 10^4\ h^{-1}$ with an inlet 1-butanol/1,3-butanediol molar flow (F) of 1 mol h^{-1}. Passage of reactant in a stream of N_2 through the empty reactor did not result in any detectable conversion. The fractional conversion of 1-butanol/1,3-butanediol (X_i) was defined as

$$X = \frac{[reactant]_{i,in} - [reactant]_{i,out}}{[reactant]_{i,in}} \qquad \textbf{(4.1)}$$

where the subscripts “in” and “out” represent the concentration of reactant entering in and concentration of the product leaving out the reactor.

4.2.5 Analytical Method and Activity/Selectivity Evaluation

The reactor effluent was directly connected to an online GC gas inlet valve *via* a 1/16-inch diameter stainless steel tube. The sample line was heated (~363 K) by tape heaters and wrapped with woven fiberglass insulation to avoid reaction product

condensation and maintain the temperature in the line. The effluent was analysed by capillary GC (Perkin-Elmer Auto System XL gas chromatograph equipped with a programmed split/split less injector and FID) using a Rtx-1 (dimethyl polysiloxane) 60 m × 0.32 mm i.d., 5 μm film thickness capillary column (RESTEK) employing Turbo-Chrom Workstation Version 6.3.2 (for Windows) for data storage and manipulation. Quantitative analysis of reactant/products in the mixture was based on detailed calibration plots (not shown) where analytical repeatability was better than ±5%. Repeated reactions with different samples from the same batch of catalyst delivered conversion and selectivity values that were reproducible to within ±6%. Carbon mass balance was complete to better than ±8%.

4.2.6 Thermodynamic analysis

All the reactant and product species involved in thermodynamics were considered. Setting the inlet 1-butanol at 1 mol, product distribution at equilibrium was determined over 273-773 K at a total pressure of 1 atm. The equilibrium calculations were made using Aspen Plus ® software where Peng-Robinson fluid package and RGIBBS reactor were applied to obtain product composition under conditions of minimised Gibbs free energy.

4.3 Results and discussion

4.3.1 Thermodynamic analysis of 1-butanol dehydration

Thermodynamic analysis of the chemical reaction provides an important measure of the maximum conversion and selectivity that is possible to achieve under specific reaction conditions [30, 31]. The possible pathways in the dehydration of 1-butanol are identified in **Figure 4.3**. The initial loss of the water molecule from 1-butanol results in the formation of the target 1-butene **(I)**, which can further undergo isomerisation (to *cis*-2-butene **(II)** and *trans*-2-butene **(III)**) or sequential hydration to 2-butanol **(IV)**. *Cis*- and/or *trans*-2-butenes can easily transform into each other **(V)** and as well as 1-butene undergo hydration reactions **(VI, VII)** to form 2-butanol. Dibutyl ether (DBE) can also be obtained **(VIII)** if initially the dehydration of two 1-butanol molecules is taking place [27].

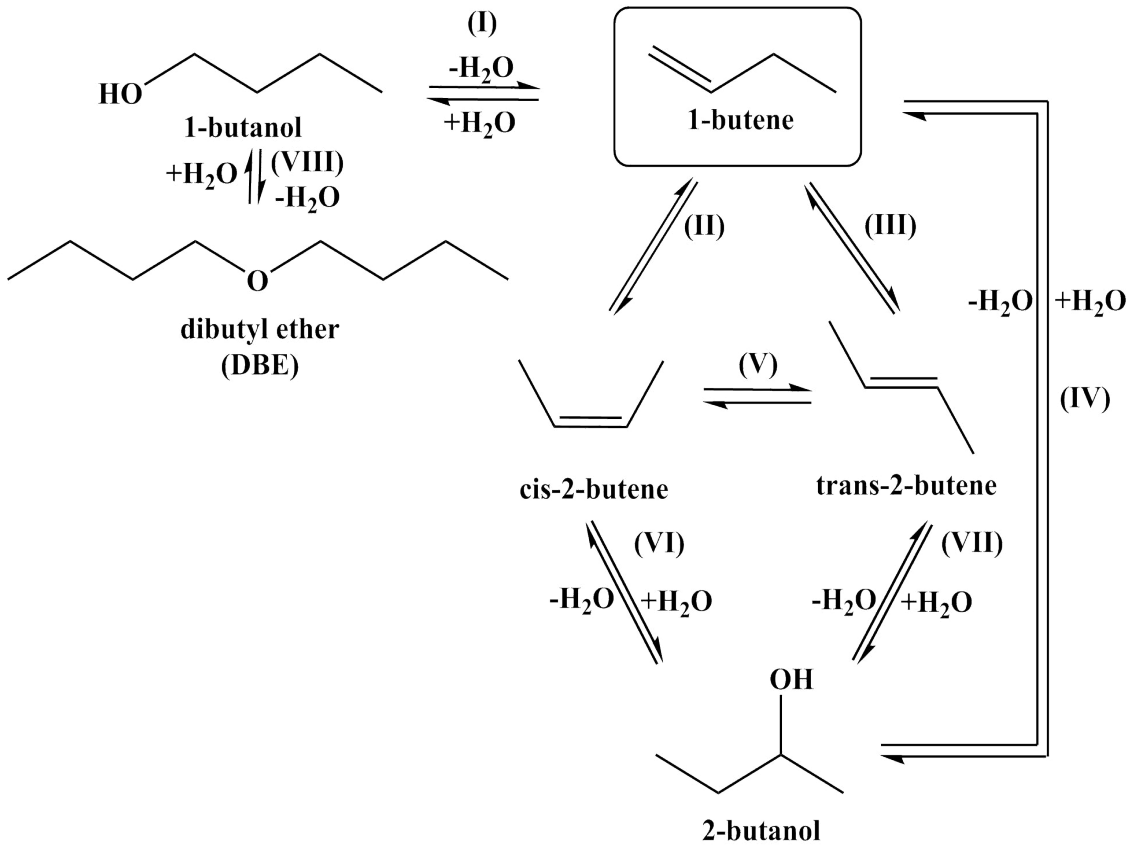

Figure 4. 3: Reaction pathways in 1-butanol dehydration.

The analysis considered the effect of reaction temperature (273 – 773 K) on the reactant conversion and product selectivity. Dehydration step was found to be fast and not rate limiting as complete 1-butanol conversion was achieved at temperatures above 323K. The effect of the temperature on product distribution has been demonstrated on **Figure 4.4**, where at low temperature range (≤400 K) a combination of 1-butene, DBE, *cis*- and *trans*-2-butenes was generated at equilibrium with *trans*-2-butene as the predominant product. An increase in temperature to 773 K resulted in a continuous decrease in selectivity to *trans*-2-butene and increase in selectivity to 1-butene. Based on this thermodynamic analysis, the reaction temperature has a negligible influence on the selectivity to DBE and *cis*-2-butene while the formation of the target 1-butene would be favoured at higher reaction temperatures.

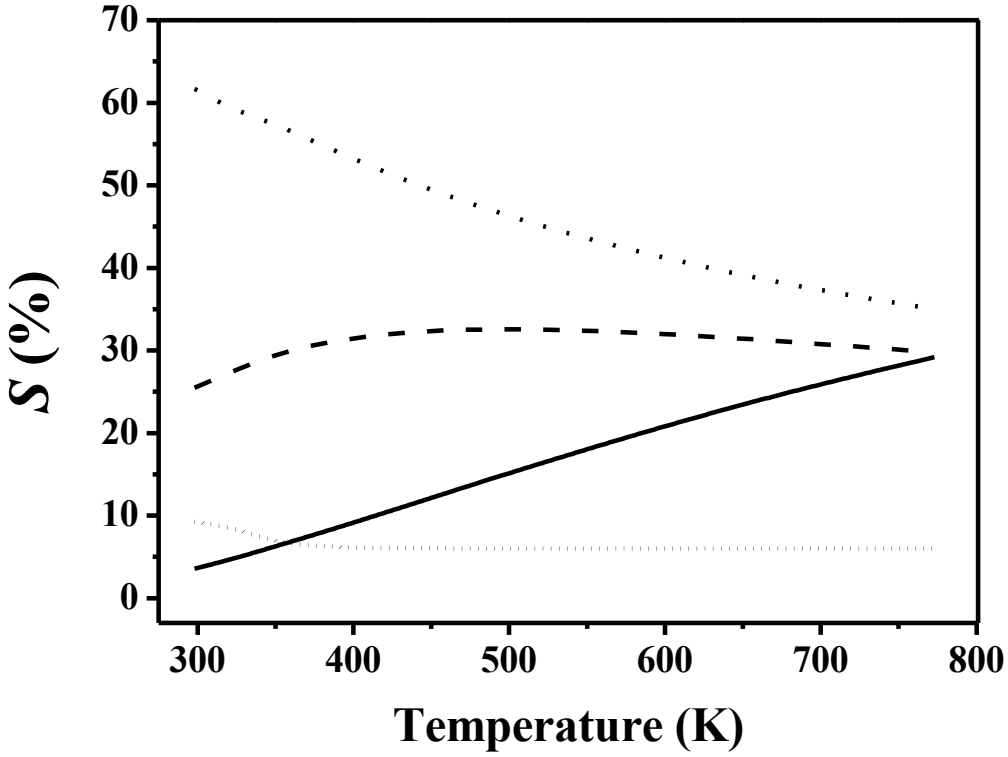

Figure 4.4: Product selectivity (*S*) as a function of temperature at the thermodynamic equilibrium: 1-butene (solid line), *cis*-2-butene (dashed line), *trans*-2-butene (dotted line) and dibutyl ether (short dotted line).

4.3.2 Catalytic Results

4.3.2.1 Dehydration of 1-butanol

Catalytic activity was assessed in terms of the fractional 1-butanol conversion (X) over CeO_2 and is presented as a function of time on-stream in **Figure 4.5(I)**. An initial temporal loss of activity was followed by the achievement of steady state conversion after 3 h on-stream. Activity profiles were fitted to the empirical relationship [32, 33].

$$\left(\frac{X - X_0}{X_{3h} - X_0}\right) = \frac{\Delta t}{\beta + \Delta t} \qquad \textbf{(4.2)}$$

where X_{3h} represents fractional conversion after 3 h on-stream and β is a time scale fitting parameter. Fit convergence yielded values for X_0, which is a measure of initial activity.

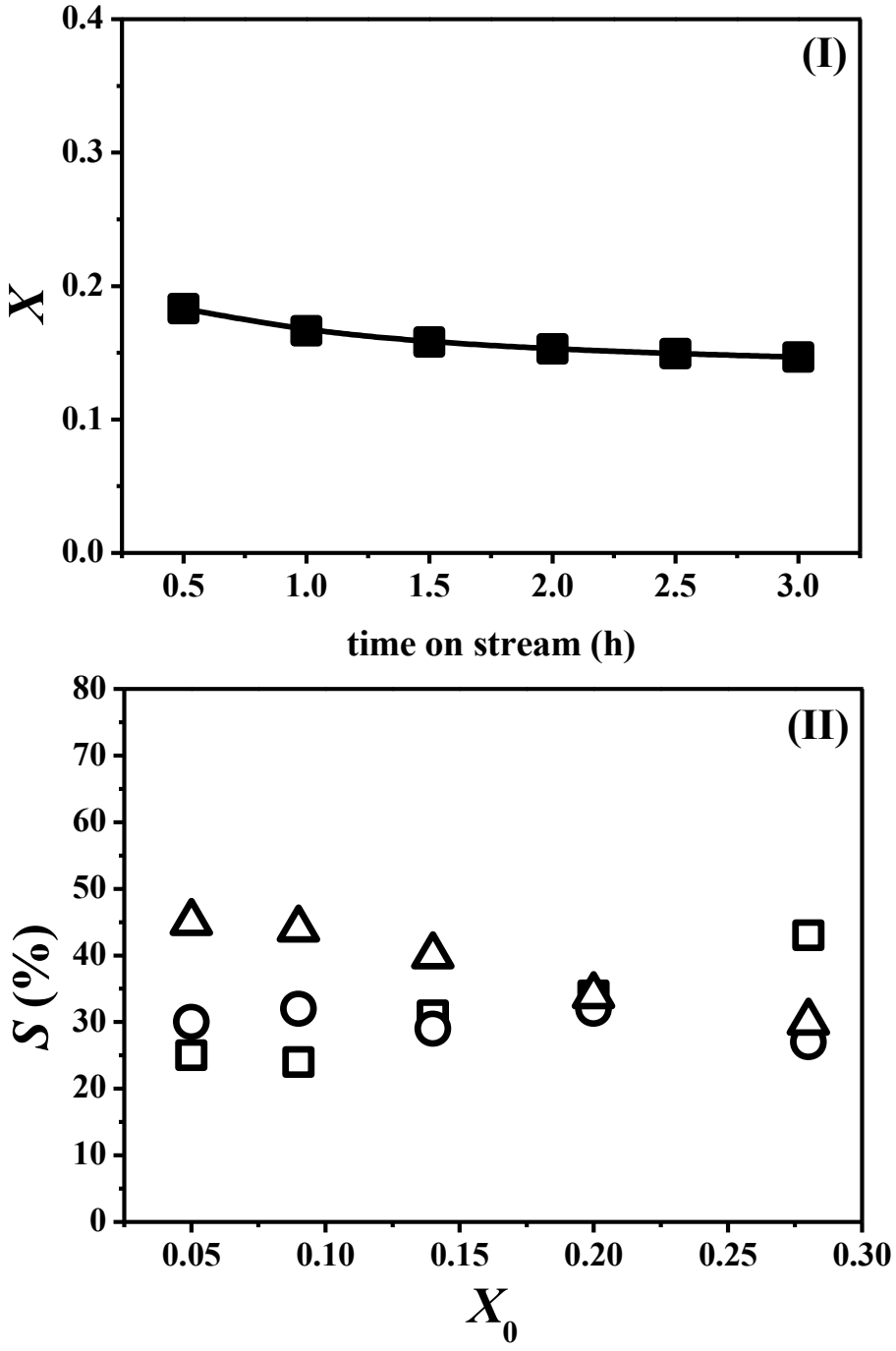

Figure 4. 5: (I) Variation of 1-butanol fractional conversion (*X*, ■) with time on stream over CeO_2; line represent fit to eq. (4.2). (II) Variation of selectivity (*S*) to 1-butene (□), DBE (○) and *cis/trans*-2-butenes (△) with initial fractional conversion of 1-butanol (X_0) over CeO_2: *T* = 473-623 K, *P* = 1 atm.

The dependence of selectivity on initial fractional conversion over CeO_2 is presented in **Figure 4.5(II)** where *cis*- and *trans*-2-butenes were combined together for easy reference. Product distribution was sensitive to conversion for reaction over CeO_2 with the mixture of 2-butene isomers as predominant products at low fractional conversion (<0.15) and a switch to a preferential 1-butene formation at higher conversion (>0.20). An activity on **Figure 4.5(II)** was raised by increasing the temperature (from 473 to 623 K) and remained far below the complete conversion that was achieved at equilibrium in the thermodynamic calculations.

The comparison of Al_2O_3 and CeO_2 was made at an equivalent fractional 1-butanol conversion (~0.2) and the results are presented in **Table 4.1**.

Table 4. 1: Product distribution and initial conversion in the conversion of 1-butanol over Al_2O_3, fresh and calcined CeO_2 at T = 573K.

Catalyst	X_0	Selectivity (%)		
		1-Butene	DBE	*(cis* and *trans)* -2-Butene
Al_2O_3	22	51	11	38
CeO_2	20	34	32	34
CeO_2 calcined	24	42	22	36

As it can be seen from the table the selectivity to the target 1-butene is higher over alumina (51 *vs.* 34%) while this difference in selectivity is mainly attributed to the formation of DBE over ceria (**Table 4.1**). It has been shown that the product formation from 1-butanol dehydration is sensitive to acid site strength [26] and 1-butene formation as well as isomerization to 2-butenes requires acid sites stronger than those involved in the DBE formation [22, 26]. The Lewis acid (LWA) strength of metal ions is proportional to the electronegativity of metals in their oxide form [34]. Al_2O_3 has higher electronegativity relative to CeO_2 (1.61 *vs.* 1.12 [35]) and, therefore, has stronger LWA sites. It has been demonstrated in the previous chapter that the calcination treatment of cerium oxide can improve the Lewis acidity of the catalyst by increasing the amount of

Ce^{4+} (LWA) species. Calcined CeO_2 was tested in dehydration of 1-butanol reaction and the results are presented in the **Table 4.1**. There was a measurable increase in the selectivity to 1-butene over calcined CeO_2 that can be linked to the decrease of weak-moderate Lewis base (LWB) sites (upon calcination), which are essential for DBE formation [26].

4.3.2.2 Dehydration of 1,3-butanediol

Dehydration of 1,3-BD can proceed *via* primary and/or secondary hydroxyl group (see **Figure 4.2**). Dehydration of 1,3-BD over Al_2O_3 resulted in a combination of 3B2OL, 3B1OL, 2B1OL and BD, where the selectivity to predominant BD was 85% and to the target 3B2OL was below 5%. Meanwhile, the switch of the catalyst to CeO_2 resulted in the formation of only 2 products: 3B2OL and 2B1OL. This means that the presence of the weak-moderate acid sites on ceria [36] helps to limit the reaction once unsaturated alcohols are produced while strong acid sites on alumina promote further dehydration of unsaturated alcohols to BD. Nevertheless, since 3B2OL and 2B1OL are produced *via* elimination of both hydroxyl groups of 1,3-BD, the mechanism of the reaction has to be considered prior further optimisation.

4.3.3 Mechanism for 1,3-butanediol dehydration

There are a few mechanisms that have been proposed for the dehydration of alcohols over CeO_2 [15, 38, 39]. The dehydration of 1,3-butanediol over CeO_2 can proceed *via* E2 (elimination of the terminal OH^-, **I**) and radical (initial reduction of Ce^{4+} site, **II**) mechanisms, which are presented in the **Figure 4.6**. The E2 dehydration mechanism (**I**) involves initial alcohol adsorption on the LWA site (Ce^{4+}) *via* terminal OH^-. The alkene is being formed and desorbed from the surface of the catalyst following by the single step β-hydrogen transfer to a surface O^{2-} and elimination of OH^-. The next step involves water formation with sequential desorption and catalyst regeneration. It should be noted that dehydration *via* E2 mechanism results in the formation of solely 3B2OL. Dehydration of 1,3-BD *via* radical mechanism (**II**) involves initial abstraction of the hydrogen atom from the second carbon with it following activation on Ce^{4+} site. Then, a hydroxyl radical is eliminated to produce an unsaturated

alcohol and water. Elimination of the terminal hydroxyl radical favours the formation of the target 3B2OL and elimination of the secondary OH favours 2B1OL.

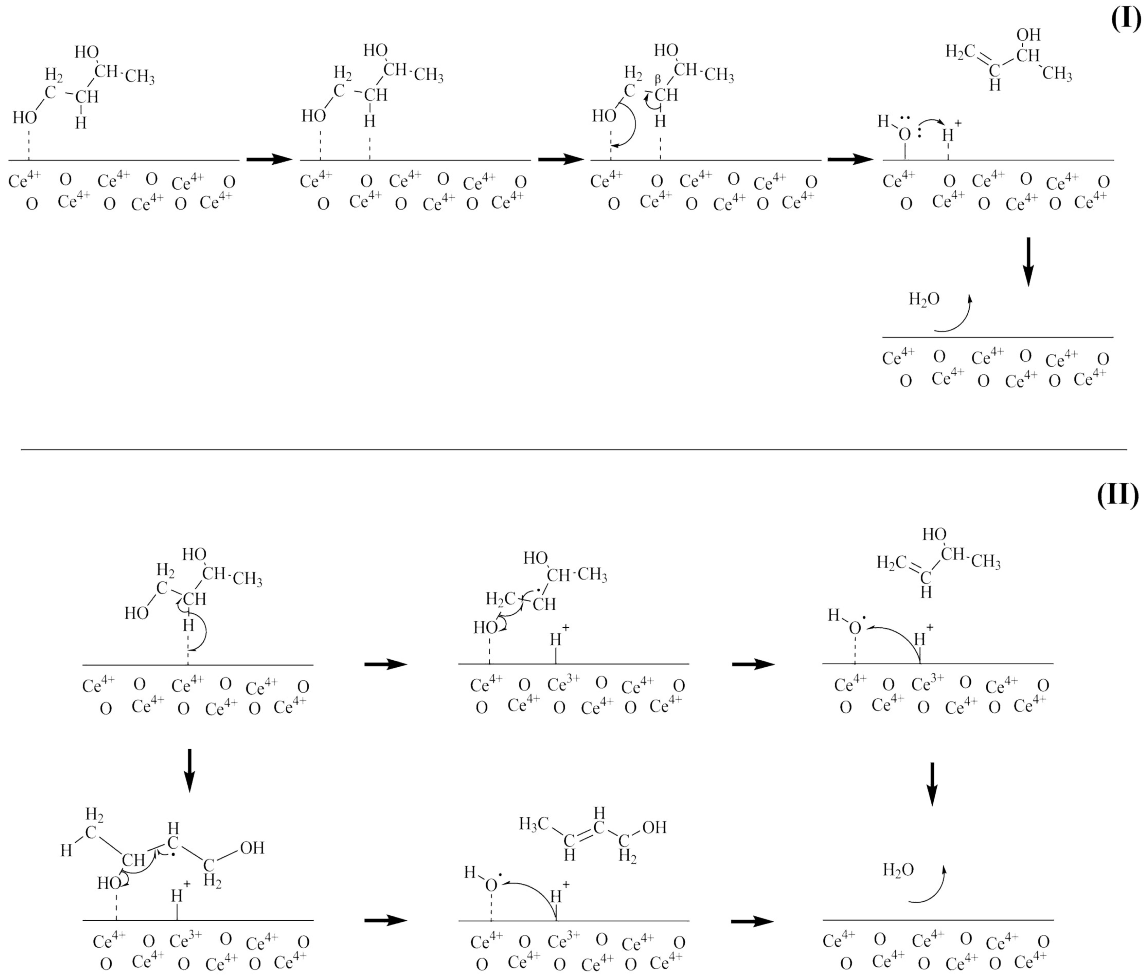

Figure 4. 6: Reaction mechanisms for the dehydration of 1,3-butanediol over CeO_2: (I) elimination of the terminal OH^- (E2) and (II) initial reduction of Ce^{4+} site (radical).

Considering these two mechanisms presented on **Figure 4.6**, the dehydration activity of CeO_2 is dependent on LWA site (Ce^{4+}) and its neighbouring LWB site (O^{2-}), while the radical mechanism requires solely Ce^{4+}. The presence of 2B1OL clearly indicates that the reaction proceed *via* mechanism (**II**), however the formation of 3B2OL can be a result of both mechanisms (**I**) and (**II**). Since mechanisms (**I**) and (**II**) require the surface Ce^{4+} sites, the reduction of CeO_2 (Ce^{4+} to Ce^{3+}) will cause the decrease in both 3B2OL and 2B1OL. Based on this, if reaction proceeds only *via* mechanism (**II**),

3B2OL/2B1OL ratio should not change during the reduction of ceria. However, if reaction is taking place *via* (**I**) together with (**III**), 3B2OL/2B1OL ratio should decrease.

4.3.4 Effect of metals

It has been previously established [40-42] that the incorporation of the noble metals (such as Au, Pd and Ag) on ceria can cause partial support reduction. Au/CeO_2, Pd/CeO_2 and Ag/CeO_2 were used in this study to promote the reduction of Ce^{4+} to Ce^{3+} and to establish the effect on 3B2OL/2B1OL ratio. Hydrogen consumption during TPR for ceria supported Au, Ag and Pd catalysts is presented in **Table 4.2**, where for all three catalysts the experimental H_2 consumption exceeded the theoretical requirement for the reduction of metal precursor.

Table 4. 2: H_2 consumption during TPR for Au/CeO_2, Pd/CeO_2 and Ag/CeO_2.

Catalyst	Au/CeO_2	Pd/CeO_2	Ag/CeO_2
Experimental H_2 consumption ($\mu mol\ g^{-1}$)	495	680	293
Theoretical H_2 consumption[a] ($\mu mol\ g_{Me}^{-1}$)	61	42	26

[a] amount required for reduction of metallic form.

The value for Pd/CeO_2 (680 $\mu mol\ g_{Pd}^{-1}$) was measurably greater, indicative to the higher extent of ceria reduction [41]. The variation of 3B2OL/2B1OL ratio over calcined CeO_2, Au/CeO_2, Ag/CeO_2 and Pd/CeO_2 is presented on **Figure 4.7**, where it can be seen that the ratio decreased in the order $CeO_2 \geq Au/CeO_2 \geq Ag/CeO_2 \geq Pd/CeO_2$. Since the decrease in Ce^{4+} content (active site of the reaction) resulted in the decrease of 3B2OL with respect to 2B1OL, we propose that the dehydration of 1,3-BD follows both E2 and radical mechanisms (**Figure 4.6, I** and **II** respectively).

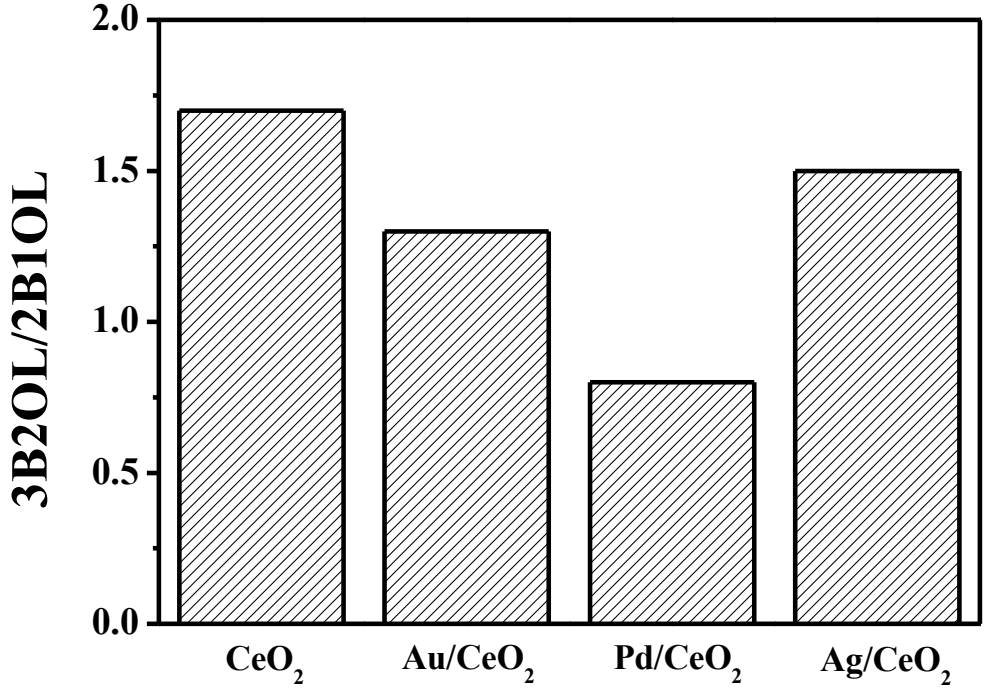

Figure 4. 7: Variation of 3-buten-2-ol/2-buten-1-ol (3B2OL/2B1OL) ratio over calcined CeO_2, Au/CeO_2, Pd/CeO_2 and Ag/CeO_2. *Reaction conditions*: T = 573 K, P = 1 atm, $X_0 \sim 0.2$.

4.4 Conclusions

Under thermodynamic control, complete conversion of 1-butanol can be achieved where an increase in temperature (to 773K) favours 1-butene formation. Dehydration of 1-butanol over both Al_2O_3 and CeO_2 delivered a product composition far removed from thermodynamic equilibrium where alumina presented the highest 1-butene selectivity (51%) due to stronger Lewis acidity. In contrast, under the same reaction conditions CeO_2 was more selective to DBE. The calcination of CeO_2 resulted in an increase of surface Ce^{4+} species (active sites), which improved the selectivity to 1-butene (from 34 to 42%). In dehydration of 1,3-BD, Al_2O_3 was not selective to the target 3B2OL since strong acid sites (Al^{3+}) promoted further dehydration to produce BD. Meanwhile, CeO_2 delivered only 3B2OL and 2B1OL as a products and two mechanisms were considered to clarify product distribution. It was established that reaction can proceed solely *via* radical or with contribution of E2 mechanisms. The incorporation of the metal on ceria

promoted a partial (Ce^{4+} to Ce^{3+}) reduction during TPR and resulted in change of 3B2OL and 2B1OL ratio. The trend observed suggest that the higher the extent of ceria reduction, the lower is the 3B2OL/2B1OL ratio, indicating that dehydration of 1,3-BD follows both E2 and radical mechanisms.

4.5 References

[4.1] S. Sato, F. Sato, H. Gotoh and Y. Yamada, *Selective Dehydration of Alkanediols into Unsaturated Alcohols over Rare Earth Oxide Catalysts*. ACS Catal., 2013. **3**: p. 721-734.

[4.2] P. R. Stapp, *Alkenol Production*. US Patent 3960972 A, 1976.

[4.3] P. R. Stapp, *Alkenol Production*. US Patent 4081486 A, 1978.

[4.4] G. Sánchez, J. Friggieri, C. Keast, M. Drewery, B.Z. Dlugogorski, E. Kennedy and M. Stockenhuber, *The Effect of Catalyst Modification on the Conversion of Glycerol to Allyl Alcohol*, Appl. Catal., B, 2014. **152-153**: p. 117-128.

[4.5] I. E. Levine and Jr W.G.Toland, *Production of Methyl Vinyl Ketone*. US Patent 2464244 A, 1949.

[4.6] S. Satoshi, Y. Katsushige, S. Satoshi and D. Hailing, *Method for Producing 1,3-Butadiene and/or 3-Buten-2-ol*. US Patent 0221904 A1, 2016.

[4.7] O. Faroon, N. Roney, J. Taylor, A. Ashizawa, M.H. Lumpkin and D.J. Plewak, *Acrolein Environmental Levels and Potential for Human Exposure*. Toxicol. Ind. Health, 2008. **24**: p.543 - 564.

[4.8] J. L. Callahan, R. K. Grasselli, E. C. Milberger and H. A. Strecker, *Oxidation and Ammoxidation of Propylene over Bismuth Molybdate Catalyst*. Ind. Eng. Chem. Prod. Res. Dev., 1970. **9**: p. 134–142.

[4.9] H. Koempel and W. Liebner, *Lurgi's Methanol To Propylene (MTP®) Report on a Successful Commercialisation*. Stud. Surf. Sci. Catal., 2007. **167**: p. 261-267.

[4.10] D. Wallenstein and R.H. Harding, *The Dependence of ZSM-5 Additive Performance on the Hydrogen-Transfer Activity of the REUSY Base Catalyst in Fluid Catalytic Cracking*, Appl. Catal., A, 2001. **214**: p. 11-29.

[4.11] W. K. Chwang, P. Knittel, K. M. Koshy and T. T. Tidwell, *Kinetics of Acid-Catalyzed Hydration of 1,3-Butadienes and Vinyl Halides. Correlation of the Reactivity of Vinyl Alkenes and Aryl Alkenes*, J. Am. Chem. Soc., 1977. **99**: p. 3395–3401.

[4.12] H. Duan, D. Sun, Y. Yamada and S. Sato, *Dehydration of 2,3-Butanediol into 3-Buten-2-ol Catalyzed by ZrO_2*, Catal.Commun., 2014. **48**: p. 1-4.

[4.13] W. Kim, W. Shin, K. J. Lee, H. Song, H. S. Kim, D. Seung and I. N. Filimonov, *2,3-Butanediol Dehydration Catalyzed by Silica-Supported Sodium Phosphates*, Appl. Catal., A, 2016. **511**: p. 156-167.

[4.14] H. Gotoh, Y. Yamada and S. Sato, *Dehydration of 1,3-Butanediol over Rare Earth Oxides*, Appl. Catal., A, 2010. **377**: p. 92-98.

[4.15] N. Ichikawa, S. Sato, R. Takahashi and T. Sodesawa, *Catalytic Reaction of 1,3-Butanediol over Solid Acids*, J. Mol. Catal. A: Chem., 2006. **256**: p. 106-112.

[4.16] S. Sato, R. Takahashi, T. Sodesawa, A. Igarashi and H. Inoue, *Catalytic Reaction of 1,3-Butanediol over Rare Earth Oxides*, A Appl. Catal., A, 2007. **328**: p. 109-116.

[4.17] K. Sakurai, Y. Miyake and T.Amagai, Reliable Passive-Sampling, *Method for Determining Outdoor 1,3-Butadiene Concentrations in Air*, Atmos. Environ.,

2013. **80**: p. 198-203.

[4.18] F. Kramp and S. E. Paulson, *The Gas Phase Reaction of Ozone with 1,3-Butadiene: Formation Yields of Some Toxic Products*, Atmos. Environ., 2000. **34**: p. 35-43.

[4.19] A.-P. Zeng and W. Sabra, *Microbial Production of Diols as Platform Chemicals: Recent Progresses*, Curr. Opin. Biotechnol., 2011. **22**: p. 749-757.

[4.20] X. Tang, J. Wei, N. Ding, Y. Sun, X. Zeng, L. Hu, S. Liu, T. Lei and L. Lin, *Chemoselective Hydrogenation of Biomass Derived 5-Hydroxymethylfurfural to Diols: Key Intermediates for Sustainable Chemicals, Materials and Fuel*s, Renew. Sust. Energ. Rev., 2017. **77**: p. 287-296.

[4.21] S. Sato, R. Takahashi, T. Sodesawa, N. Honda and H. Shimizu, *Selective Dehydration of Diols to Allylic Alcohols Catalyzed by Ceria*, Catal. Commun., 2003. **4**: p. 77-81.

[4.22] H. Metiu, S. Chrétien, Z. Hu, B. Li and X. Sun, *Chemistry of Lewis Acid-Base Pairs on Oxide Surfaces*, J. Phys. Chem. C, 2012. **116**: p. 10439–10450.

[4.23] E. Iglesia, D. G. Barton, J. A. Biscardi, M. J. L. Gines and S. L. Soled, *Bifunctional Pathways in Catalysis by Solid Acids and Bases*, Catal. Today, 1997. **38**: p. 339–360.

[4.24] S. Roy, G. Mpourmpakis, D.-Y. Hong, D. G. Vlachos, A. Bhan and R. J. Gorte, *Mechanistic Study of Alcohol Dehydration on γ-Al_2O_3*, ACS Catal., 2012. **2**: p. 1846–1853.

[4.25] G. R. Jenness, M. A. Christiansen, S. Caratzoulas, D. G. Vlachos and R. J. Gorte, *Site-Dependent Lewis Acidity of γ-Al_2O_3 and Its Impact on Ethanol Dehydration and Etherification*, J. Phys. Chem. C, 2014. **118**: p. 12899–12907.

[4.26] F.M. Bautista and B. Delmon, *1-Butanol Dehydration on $A1PO_4$ and Modified $A1PO_4$: Catalytic Behaviour and Deactivation*, Appl. Catal., A, 1995. **130**: p. 47-65.

[4.27] S. Delsarte and P. Grange, *Butan-1-ol and Butan-2-ol Dehydration on Nitrided Aluminophosphates: Influence of Nitridation on Reaction Pathways*, Appl. Catal., A, 2004. **259**: p. 269-279.

[4.28] W.-J. Shen and Y. Matsumura, *Interaction Between Palladium and The Support in Pd/CeO_2 Prepared by Deposition–Precipitation Method and The Catalytic Activity for Methanol Decomposition*, J. Mol. Catal. A: Chem., 2000. **153**:p. 165-168.

[4.29] F. Cárdenas-Lizana, S. Gómez-Quero, C. Amorim and M.A. Keane, *Gas Phase Hydrogenation of p-Chloronitrobenzene over $Pd–Ni/Al_2O_3$.* Appl. Catal., A, 2014. **473**: p. 41-50.

[4.30] X. Wang, S. Li, H. Wang, B. Liu and X. Ma, *Thermodynamic Analysis of Glycerine Steam Reforming*, Energy Fuels, 2008. **22**: p. 4285-4291.

[4.31] X. Wang, M. Li, M. Wang, H. Wang, S. Li, S. Wang and X. Ma, *Thermodynamic Analysis of Glycerol Dry Reforming for Hydrogen and Synthesis Gas Production*, Fuel, 2009. **88**: p. 2148-2153.

[4.32] K.V. Murthy, P.M. Patterson and M.A. Keane, *C–X Bond Reactivity in the Catalytic Hydrodehalogenation of Haloarenes over Unsupported and Silica Supported Ni*. J. Mol. Catal. A: Chem., 2005. **225**: p. 149-160.

[4.33] S. Jujjuri, E. Ding, E. Hommel, S. Shore and M.A. Keane, *Synthesis and Characterization of Novel Silica-Supported Pd/Yb Bimetallic Catalysts:*

Application in Gas-Phase Hydrodechlorination and Hydrogenation. J. Catal., 2006. **239**: p. 486-500.

[4.34] I. D. Brown and A. Skowron, *Electronegativity and Lewis Acid Strength*, J. Am. Chem. Soc., 1990. **112**: p. 3403-3408.

[4.35] W. Gordy and W.J. Thomas, *Electronegativities of the Elements*, J. Chem. Phys., 1956. **24**: p. 439.

[4.36] E. Leino, N. Kumar, P. Mäki-Arvela, A. Aho, K. Kordás, A.-R. Leino, A. Shchukarev, D.Y. Murzin and J.-P. Mikkola, *Influence of the Synthesis Parameters on the Physico-Chemical and Catalytic Properties of Cerium Oxide for Application in the Synthesis Of Diethyl Carbonate.* Mater. Chem. Phys., 2013. **143**: p. 65-75.

[4.37] S. Sato, R. Takahashi, T. Sodesawa and N. Honda, *Dehydration of Diols Catalyzed by CeO_2*, J. Mol. Catal. A: Chem., 2004. **221**: p. 177−183.

[4.38] N. Ichikawa, S. Sato, R. Takahashi, T. Sodesawa, H. Fujita, T. Atoguchi and A. Shiga, *Theoretical Investigation of 1,3-Butanediol Adsorption on an Oxygen-Defected CeO_2(111) Surface*, J. Catal., 2006. **239**: p. 13–22.

[4.39] T. Nozawa, S. Sato and R. Takahashi, *Vapor-Phase Dehydration of 1,3-Butanediol over CeO_2–ZrO_2 Catalysts*, Top. Catal., 2009. **52**: p. 609–617.

[4.40] D. Andreeva, V. Idakiev, T. Tabakova, L. Ilieva, P. Falaras, A. Bourlinos and A.Travlos, *Low Temperature Water-Gas Shift Reaction over Au/CeO_2 Catalysts*, Catal. Today, 2002. **72**: p. 51-57.

[4.41] D.R. Mullins, *The Surface Chemistry of Cerium Oxide*, Surf. Sci. Rep., 2015. **70**: p. 42-85.

[4.42] H. Zhang, A. Zhu, X. Wang, Y. Wang and C. Shi, *Catalytic Performance of Ag–Co/CeO_2 Catalyst in NO–CO and NO–CO–O_2 System*, Catal. Commun., 2007. **8**: p. 612-618.

Chapter 5

Summary and Future Work

5.1 General Conclusions

The main objective of this thesis was to explore alternative cleaner routes for the sustainable production of valuable oxygen containing compounds with multiple industrial applications. This work has focused on the use of ceria-based catalysts with detailed characterisation to allow correlation of structure with performance. Reaction mechanisms underpinning each process have also been considered. The significant findings of this work are provided in this Chapter and future research directions are proposed. In the gas phase transformation of LA to GVL, presented in **Chapter 2**, the nature of the support (reducible *vs. non*-reducible) has a considerable impact on catalytic performance. The Al_2O_3 supported Pd exhibited the highest LA consumption rate among all of the catalysts studied but generated an undesirable pentanoic acid as a by-product. This work has tackled selectivity issues, taking a series of approaches directed at maximising exclusive formation of a target GVL by decreasing the H_2 feed content and introducing the supported Au systems. It was concluded that the surface oxygen vacancies generated during TPR for Au on reducible supports (CeO_2 and TiO_2) promote the activation of LA and elevate the overall reaction rate. The reducibility of CeO_2 was further investigated in **Chapter 3**, where a comparison of the catalytic action of Pd/CeO_2, commercial and synthesised CeO_2 catalysts served to establish the involvement of surface Ce^{4+} and Ce^{3+} in carbonate/carbamate production. Comparison of the continuous gas phase and liquid batch modes of operation has established clear advantages for the former in terms of activity due to more efficient removal of co-produced water from the surface of the catalyst. The characterisation and catalytic results demonstrate that calcination treatment of CeO_2 increased Ce^{4+} content with a

concomitant decrease in surface area and increase in particle size. It was concluded that higher Ce^{4+}/Ce^{3+} ratio and the presence of surface O^{2-} promote the CO_2 activation. Contact time is an essential process variable where the use of multiple catalyst beds in series facilitates enhanced product output. Carbamate was achieved over a double-bed (CeO_2 on top and Pd/CeO_2 on the bottom) arrangement. Modification of surface $Ce^{3+} \rightarrow Ce^{4+}$ of CeO_2 caused the decline of weak-moderate surface basicity that was mainly attributed to Ce^{3+} sites. The acid-base character of CeO_2 plays a critical role and it was further examined in **Chapter 4**, where Lewis acid (LWA) sites are rate determining in the dehydration of mono- and polyalcohols into corresponding alkenes. A comparison between Al_2O_3 and CeO_2 revealed that stronger LWA sites are preferential for the formation of the target alkene while weaker LWB sites are essential for etherification. It was established that dehydration can proceed *via* initial elimination of the hydroxyl group of an alcohol or *via* elimination of a β-hydrogen radical on the LWA site (Ce^{4+}). The incorporation of metals promoted a partial (Ce^{4+} to Ce^{3+}) reduction during TPR and caused distinct product distribution that was in agreement with the presented mechanisms.

5.2 Future Directions

5.2.1 Selective Transformation of Succinic Acid to γ-Butyrolactone

The work presented in **Chapter 2** has established that the redox properties of CeO_2 significantly enhance the rate of GVL production by means of LA activation at surface oxygen vacancies. An extension of the work to more complex reactions that involve carbonyl group transformation is essential to support these findings. For instance, investigating the selective hydrogenation of succinic acid to γ-butyrolactone, which is an important chemical intermediate and solvent in fine chemical and pharmaceutical industries [1, 2]. The majority of the work has been conducted in batch liquid phase operation under high pressures (>50 bar) and with low yields of the target product

(<50%) [3]. Exclusive production of γ-butyrolactone is challenging due to cyclisation/dehydration and hydrogenation reactions, which require a catalyst with emphasised acid properties and hydrogenation activity [4]. Drawing on the selective catalytic action of Au/CeO_2 in C=O reduction (**Chapter 2**) a programme of study is proposed to examine the role of support in hydrogenation of succinic acid over Au.

5.2.2 Catalytic Dehydration of 2,3-Butanediol to 3-Buten-2-ol over Ceria

As established in **Chapter 4**, dehydration of 1,3-butanediol over the range of ceria-based catalysts results in the formation of two specific unsaturated alcohols, target 3-buten-2-ol and by-product 2-buten-1-ol. The modification of surface chemistry of CeO_2 by calcination treatment or metal incorporation caused the change in proportion between these products. This reaction system requires further exploration. It is proposed to extend the dehydration work with the use of 2,3-butanediol as reactant. This would eliminate the formation of unfavoured 2-buten-1-ol since both hydroxyl groups are not in the terminal position. There is evidence in the literature that the acid-base properties of CeO_2 can alter the product distribution [5]. The continuous gas phase dehydration of alkanediols over ceria-based catalysts requires further investigation.

5.3 References

[5.1] C. Gao, Y. Zhao and D. Liu, *Liquid Phase Hydrogenation of Maleic Anhydride over Nickel Catalyst Supported on ZrO_2–SiO_2 Composite Aerogels*. Catal. Lett., 2007. **118**: p. 50-54.

[5.2] C. Zhang, L. Chen, H. Cheng, X. Zhu and Z. Qi, *Atomically Dispersed Pd Catalysts for the Selective Hydrogenation of Succinic Acid to γ-Butyrolactone*. Catal. Today, 2016. **276**: p. 55-61.

[5.3] A. Corma, S. Iborra and A. Velty, *Chemical Routes for the Transformation of Biomass into Chemicals*. Chem. Rev., 2007. **107**: p. 2411-2502.

[5.4] U.G. Hong, S. Hwang, J.G. Seo, J. Lee and I.K. Song, *Hydrogenation of*

Succinic Acid to γ-Butyrolactone (GBL) over Palladium Catalyst Supported on Alumina Xerogel: Effect of Acid Density of the Catalyst. Ind. Eng. Chem. Res., 2011. **17**: p. 316-320.

[5.5] S. Sato, F. Sato, H. Gotoh and Y. Yamada, *Selective Dehydration of Alkanediols into Unsaturated Alcohols over Rare Earth Oxide Catalysts*. ACS Catal., 2013. **3**: p. 721-734.